

Hydrothermal synthesis of pure nanostructured ZrO₂, Y₂O₃ doped ZrO₂ and Gd₂O₃ doped ZrO₂ ceramic biomaterials and certain characterization methods

A Master's Thesis submitted for the degree of
“Master of Science”

supervised by
Prof. Dipl.-Ing. Dr.techn. Ilie Gebeshuber

Simona-Elena Bejan, PhD

12038045

Affidavit

I, **SIMONA-ELENA BEJAN, PHD**, hereby declare

1. that I am the sole author of the present Master's Thesis, "HYDROTHERMAL SYNTHESIS OF PURE NANOSTRUCTURED ZRO₂, Y₂O₃ DOPED ZRO₂ AND GD₂O₃ DOPED ZRO₂ CERAMIC BIOMATERIALS AND CERTAIN CHARACTERIZATION METHODS", 67 pages, bound, and that I have not used any source or tool other than those referenced or any other illicit aid or tool, and
2. that I have not prior to this date submitted the topic of this Master's Thesis or parts of it in any form for assessment as an examination paper, either in Austria or abroad.

Vienna, 11.04.2022

Signature

Hydrothermal synthesis of pure nanostructured ZrO_2 , Y_2O_3 doped ZrO_2 and Gd_2O_3 doped ZrO_2 ceramic biomaterials and certain characterization methods

ACKNOWLEDGEMENTS

Completing this study program and the master thesis could not have been possible without the expertise, dedication, patience, and keen interest of Associate Prof. Dipl.-Ing. Dr.techn. Ilie Gebeshuber – the adviser of this thesis, and Professor Emeritus Peter Kopacek (aka Papa Smurf) – the one responsible for me studying the Master's program in Engineering Management.

I would also like to thank Dr. Eng. Roxana-Mioara Piticescu, General Manager at National Research & Development Institute for Nonferrous and Rare Metals – IMNR (Romania), for allowing me to use the infrastructure of the Advanced and Nanostructured Materials Laboratory to obtain the materials.

I am owing a debt of gratitude to Dr. Eng. Alina-Mihaela Melinescu - Associate Professor at the Politehnica University of Bucharest - Department of Science and Engineering of Oxide Materials and Nanomaterials; and to Petre-Cristian Mitroi – studying a master program on Chemistry of Advanced Materials at Faculty of Chemistry - the University of Bucharest, for their support in interpretation the results of characterization methods for the obtained ceramic materials.

A special "Thank you!" to my dearest friends and colleagues, Ioana Vlaicu, Carolina Castellanos, and Mihnea Popa, the ones that were there for me on my not-so-good days – at work, studies, and at the end of the day to cheer and motivate me.

Last but not least, I would like to thank my mom, Elena Dascalu – without you, none of this would indeed be possible; and my dad, Dumitru Bejan – pretty sure you are proud of me there, in the afterlife.

Abstract

This thesis aims to successfully synthesize nanostructured powders of simple / pure zirconia and rare-earth-doped zirconia, with a Rare Earth Oxide (REO) based content of 5 wt% molar (REO = Y_2O_3 and Gd_2O_3). The role of rare earth elements as dopants is to stabilize the zirconia, preferably in the tetragonal form.

The proposed method is hydrothermal synthesis, due to its efficiency regarding time, energy consumption, costs of materials, eco-friendliness, but most of all due to the considerable amount of ceramic nanopowders obtained, compared to other obtaining methods like sol-gel, co-precipitation, calcination or atmospheric plasma spraying.

The samples are characterized using various techniques, such as X-ray diffraction for the crystal structure, Scanning Electron Microscopy and EDX for morphology, and Fourier-Transform Infrared spectroscopy (FTIR) for surface chemistry. Each technique is described in the chapter dedicated to Materials and Methods.

The obtained results are comparable to the existing data from the literature.

Table of contents

Acknowledgements	
Abstract	I
Chapter 1. Biomaterials – general aspects	1
1.1. Introduction	1
1.2. Design and manufacturability	5
1.3. Mechanical properties	7
1.4. Ceramics	7
Chapter 2. Zirconia	8
2.1. General aspects	8
2.2. Zirconia physical properties	9
2.3. Zirconia mechanical properties	13
2.4. Zirconia stability	14
2.5. Zirconia radioactivity	16
Chapter 3. Materials and methods	17
3.1. Hydrothermal synthesis	17
3.2. Characterization methods	26
3.2.1. SEM	26
3.2.2. EDX	30
3.2.3. FTIR	30
3.2.4. XRD	31
Chapter 4. Results and discussions	34
4.1. FTIR analysis	34
4.2. XRD characterization	38
4.3. SEM and EDX analysis	41
Chapter 5. Conclusions	51
List of abbreviations	53
List of figures	54
List of tables	56
Bibliography	57

Chapter 1

Biomaterials – General aspects

1.1. Introduction

It may happen in different situations where organs and human tissues cannot perform at their best, which is caused by age, illness or injuries, and genetic defects.

Some of these conditions are handled using a daily medication, i.e., drugs. Nonetheless, some of them cannot be treated/repared only by medication, devices, and materials with specific properties required. These lead to unavoidable surgical repairs involving anatomical parts such as knee joints, vertebrae, elbow joints, teeth, and the most important organs such as the heart, kidneys, skin, etc. In a broader perspective, materials presenting unique characteristics or properties that can be used to repair, replace, or treat human and mammal tissues and/or organs are named biomaterials. Such biomaterials are formed directly from nature or can be obtained using physical or chemical processes. Research teams like Cooke's (Cooke et al. 1996), Ratner (1996), Ramakrishna's (Ramakrishna et al. 2010), and Marin's (Marin et al. 2020) contributed to broadening the multidisciplinary applications of biomaterials, interconnecting in time several fields of study (Figure 1.1). In order to design a simple biomaterial, interdisciplinary knowledge is required. It needs the synergistic integration of knowledge in materials, biology, medicine, mechanical sciences, and chemistry.

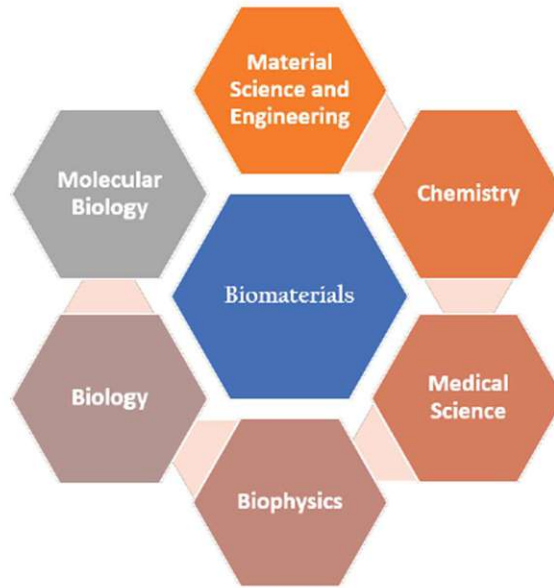


Figure 1.1. Interdisciplinary system of biomaterials (Marin et al., 2020).

The word “biomaterials” generally describes all the materials that repair or replace specific functions within/inside humans or animals and do not cause any issues like toxic reactions. This description makes the difference between biomaterials and any other type of material based on its ability to be in contact with human body tissues without causing any unwanted reaction or response. For thousands of years, people tried and succeeded in using materials to create practical devices and instruments by obtaining them from certain elements and chemical substances.

Over time, biomaterials were used in medicine, their evolution being observed gradually. The broad definition has been improved over the years and could be further expanded to new applications in emerging medicine, based on how biomaterials developed in time. Lately, scientists have reached a consensus on defining biomaterials as “a material designed to take a form that can direct, through interactions with living systems, the course of any therapeutic or diagnostic procedure” (Williams, 2019).

A biomaterial is generally either natural or synthetic biocompatible material used to wholly partially replace or support organs or tissues in close contact with other living tissues. The used materials are found in various forms such as liquid, solid, and gel (metals, polymers, ceramics, and composites). (Kranthi and Ramakrishna, 2021)

It is to be mentioned that the prefix “bio” contained in the word biomaterials refers to biocompatibility instead of biological or biomedical. The domain of biomaterials, due

to its interdisciplinarity is part of the development of quality of life and human status, because it relates to various health-related issues.

Recently, applications of Biomaterials have developed from medical devices (surgical tools) and diagnostics (biosensors) to medications used in therapy (medical implants) and drugs used in regeneration (tissue-engineered skin). Classification of both natural and synthetic medicinal materials was completed by several scientists and their teams regarding the place and role of those materials in the human body: skeletal system (fractures and defects of bones, dental implants, joint replacements, and artificial tendons and ligaments) (Cooke et al. 1996), cardiovascular system (blood vessel prosthesis, heart valves) (Kuhn, 2005), organs (artificial heart, skin repair) (Ratner et al.2020), Etc. The vital applications are presented in Figure 1.2 and tabulated in Table 1.1.

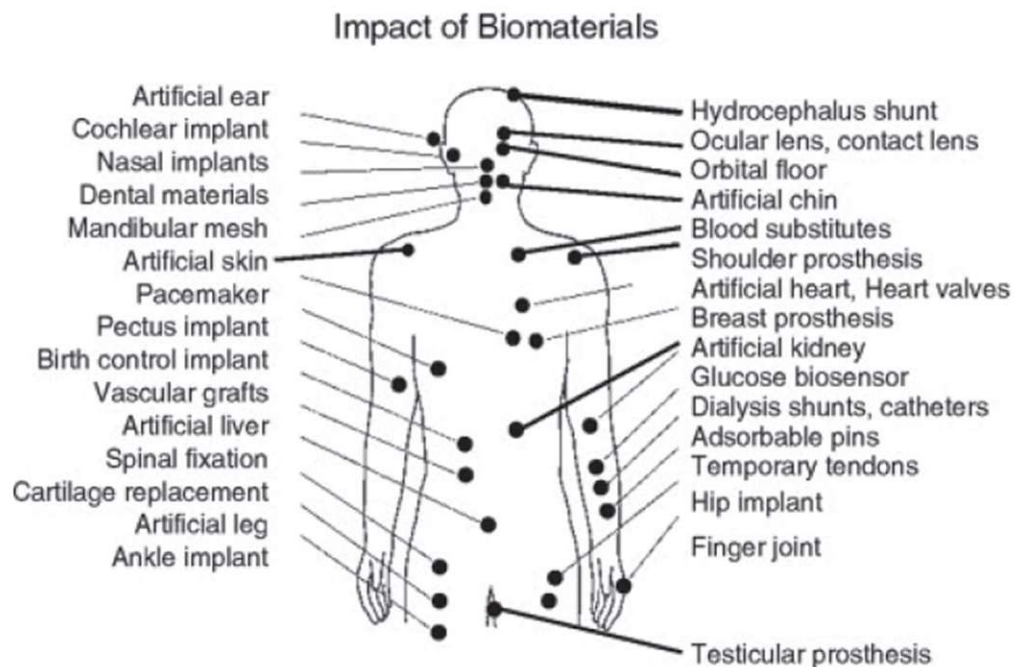


Figure 1.2: Biomaterials played a significant role in injury and disease treatment (Ratner *et al.*, 2020).

When choosing a biomaterial for a specific application, both the chemical and mechanical characteristics of the biological system must be taken into account so that the wanted functional result is fulfilled (Figure 1.3). In addition, different elements from science and social parameters are also considered for processing biomaterials and related medical items.

Table 1.1: Applications of biomaterials. (Kiran 2021)

Organ / Tissue / Joint / Bone	Examples
Heart	Biventricular pacemakers, artificial valves, artificial heart
Eye	Contact lens, artificial intraocular lens
Ear	Hair-clip artificial stapes, cochlear implants
Muscle	Sutures
Kidney	Dialysis machines
Skin	Skin wound repair, burn dressings, skin substitutes, artificial skin
Circulation	Synthetic blood vessels
Bone	Bone screws, plates, pins, intramedullary rods, bone cement to repair defects
Teeth	Fillings and replacements

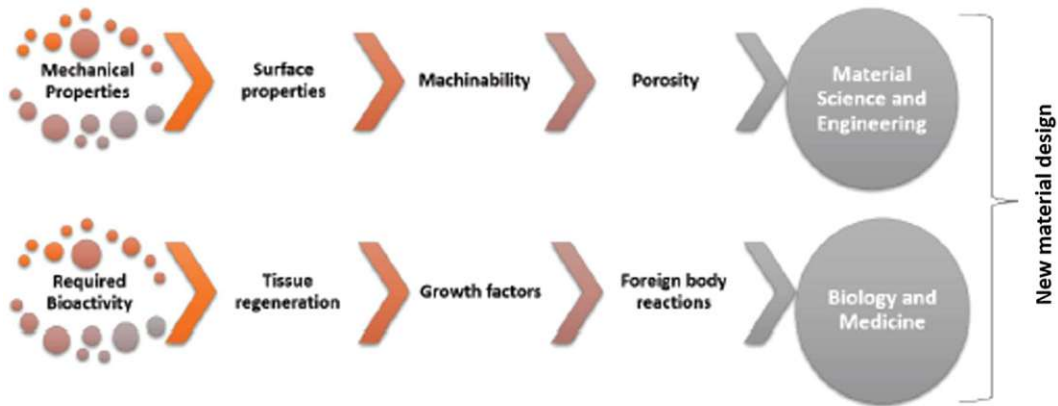


Figure 1.3: Primary requirements of new material design. (Kiran, 2021)

Regarding the biological aspect, biocompatibility refers to accepting synthetic or natural non-living materials that exist in a living human body. Williams and his team (Williams 2008) defined this acceptance as the material ability to “perform its desired functions concerning a medical therapy” and furthermore, “to induce an appropriate host response (...) and to interact with living systems without having a risk of injury, toxicity, or rejection by the immune system (...).” Generally, the biocompatibility criteria vary for each individual and medical application. For example, it may happen that the composition of materials used successfully in implantology is optimal for surgery and medical prosthetics but less effective for biocompatibility in skin-related applications.

1.2. Design and manufacturability

The most crucial factor to be considered when creating a biomaterial is the proper design of material composition. For example, in the early 1900s, bone plates were utilized to fix long bone fractures. One of the first primitive designs was not considered the mechanical properties effectively. The less fortunate result ended up in ruptured experimental plates because of the stress-focusing corner and their narrowness. The ability to efficiently manufacture the component to fit and be cost-effective while providing high reliability is called manufacturability. Concerning biomaterials, the manufacturability, in a broader sense, incorporates the material's potential to be sterilized by a validated sterilization technique that is deemed appropriate for biomedical applications. It is desirable that the material not be affected by techniques such as dry heat, autoclaving, or radiation.

It results that a biomaterial must fulfill the following specifications:

- to be biocompatible, to not present any toxic, carcinogenic, or allergenic issues
- to present the needed physical and chemical characteristics
- to present convenient mechanical properties
- to present endurance for the needed time
- to be quickly processed with the feasible techniques
- to be easy to sterilize with current facilities without any difficulty
- be affordable and available

Based on chemical bonding, materials can be classified as polymers, ceramics and metals. However, due to their different structures given by the covalent, ionic, or metallic bonds, they present different properties and applications in the body. Therefore, a new group should be considered when discussing biomaterials – lipids. Even though lipids are not sizable macromolecular polymers, several are formed by different tiny molecules' chemical combinations. Therefore, each material presents advantages and disadvantages and, based on its specific properties and the intended place substitution, it is easy to choose the proper biomedical applications. Starting from a primary classification (Wagner, 2020), the four groups described above are presented in Table 1.2, gathering data from (He 2017), (Ghasemi - Mobarakeh, 2019), and (Gul 2020).

Table 1.2. The brief classification of biomaterials based on their specific properties (Wagner, 2020)

Attributes	Polymers	Lipids	Metals & Alloys	Ceramics
Types of bonds present	Covalent & van der Waals forces	Nonpolar & polar covalent	Metallic	Ionic / Covalent
Melting point	Low	Low	Intermediate	High
Chemical stability	Poor	High	Good	Very high
Electrical conductivity	Very low	Varies	High	Very low, but varies
Thermal conductivity	Very low to intermediate	Low	High	Low
Properties and advantages	Degradable, inert, similar density to soft tissues and ease of processing	Precursors for beneficial active compounds	High strength and hardness	Non-conductive and inert; closely mimic biological properties of bone
Mechanical deformation	Very high, plastic (can be easily shaped and processed)	Low	High (ductile)	Low (brittle)
Major issues	Thermally unstable; low strength	Metabolism disorders	Wear and corrosion	High density and brittle
Biomedical applications	Soft tissue implants; drug delivery systems; tissue engineering	Regulating cell homeostasis through various processes, including cell structure formation, energy storage, and cellular signaling.	Hard tissue applications (Orthopedic and dental implants)	Tissue engineering

1.3. Mechanical properties

Biocompatibility and mechanical properties are essential in the final product, when designing biomaterials. Materials experience various forces, such as stress, strain, shear, and a combination of them. In implantology, mechanical properties such as tensile strength, Young's modulus, hardness, yield strength, and corrosion essential when designing the materials. For complex tissue applications, the mechanical properties are of top priority.

1.4. Ceramics

Ceramics are inorganic solid materials consisting of metallic and nonmetallic elements predominantly bound by ionic bonds. They exist as both crystalline and non-crystalline (amorphous) compounds. Ceramics are characterized by excellent biocompatibility, corrosion resistance, wear resistance, strength, exceptional high values of stiffness, and hardness. The upgrading of ceramics in biomedical applications relates mainly to orthopedics and dentistry. The most used ceramics are alumina (Al_2O_3) and zirconia (ZrO_2) for their bioinert property and calcium phosphates for their bioresorbable property.

Chapter 2

Zirconia

2.1. General aspects

Due to its high mechanical strength and structure toughness, zirconia has good perspectives as a biomaterial. Therefore, it is highly used in orthopedics and as a dental restorative material.

When heated, undoped/pure zirconia presents an increasing density based on phase transformation, a fact that determines cracking and residual stress; for this reason, pure zirconia cannot be sintered.

Adding an oxide as a stabilizer, makes it easier to control both sintering and phase transformations. Yttrium oxide (Y_2O_3) serves as a stabilizer. (https://www.uobabylon.edu.iq/eprints/publication_12_1581_1707.pdf)

The chemical element zirconium is a metal that has been known from ancient times: the name is a derivation of the Arabic word Zargon (golden in color), which derives in turn from the Persian words Zar (Gold) and Gun (Color) (Piconi 2016). Zirconia, the metal dioxide (ZrO_2), was identified in 1789 by German chemist Martin Heinrich Klaproth and was used for a long time to give color (as pigment) to ceramics (Piconi 2016).

The development of zirconia (zirconium dioxide: ZrO_2) ceramics as a biomaterial began around 1985 by manufacturing ball heads for total hip replacements to replace alumina ceramics due to its mechanical limitations. Initially, scientists tried to develop Magnesia-Partially Stabilized Zirconia (Mg-PSZ) due to the presence of the tetragonal phase represented by a slight acicular precipitate within large cubic grains (\varnothing 40 μ m - 50 μ m) forming the matrix (Piconi 1999). Regarding the polyethylene used in the components of the hip bone prosthesis, coupled with the zirconia ball heads in total hip replacements, it is possible for this feature to impact its wear properties negatively. Therefore, scientists focused their work mainly on Yttria – Stabilized Tetragonal Zirconia Polycrystal. Y-TZP is a ceramic formed predominantly by grains measuring over 100 nm, thus becoming a standard material in medical applications. (Fig. 2.1) (Piconi 1999).

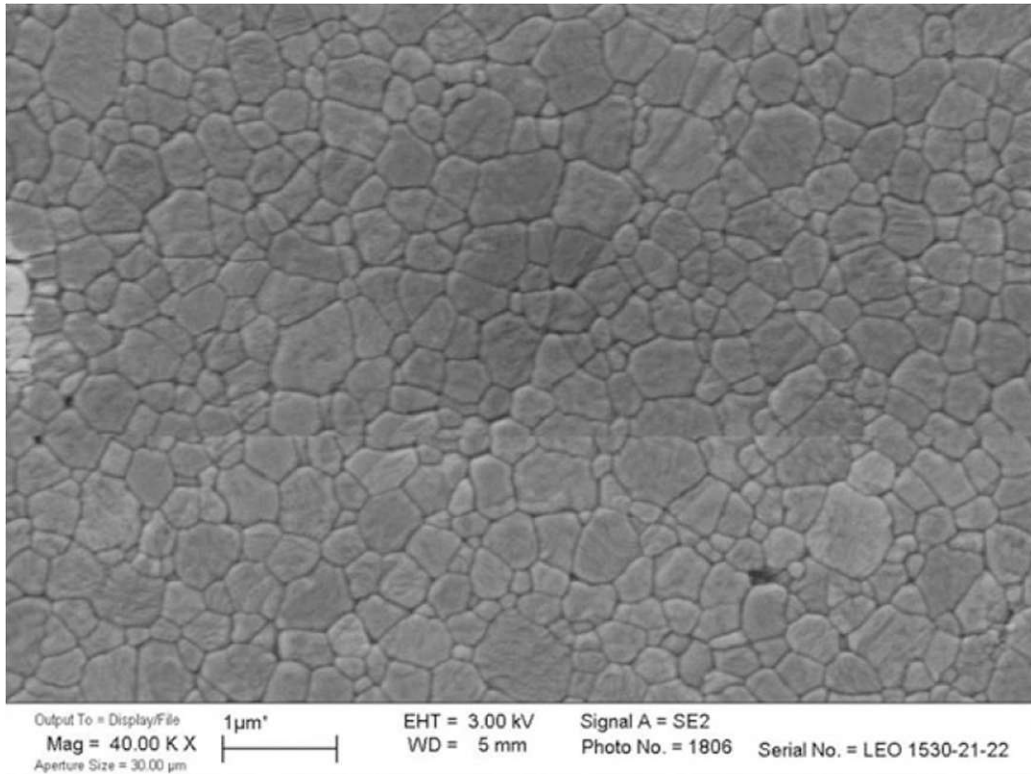


Figure. 2.1. Microstructure of Y-TZP (Courtesy of Dr. L.Pilloni, ENEA, Italy)
(Piconi 2015)

When seen in two dimensions, the tetragonal phase presents acicular crystallites. In the aging process with strict time/temperature conditions, the grains nucleate within a cubic phase if subjected to rapid cooling. These conditions become a drawback for large-scale manufacturing.

2.2. Zirconia Physical Properties

Zirconia (Zirconium dioxide, ZrO_2) is an allotropic oxide (“the existence of a chemical element in two or more forms, which may differ in the arrangement of atoms in crystalline solids or in the occurrence of molecules that contain different numbers of atoms” – as defined on [Britannica](#)), with the same chemical formula it may occur in three crystal structures – monoclinic, tetragonal, and cubic – depending on temperature. Its crystal lattice is monoclinic up to 1170°C when it shifts to tetragonal, a crystal structure that is maintained up to 2370°C . The tetragonal lattice shifts into cubic at this temperature, maintaining this form up to melting temperature (2680°C). (Piconi 2016)

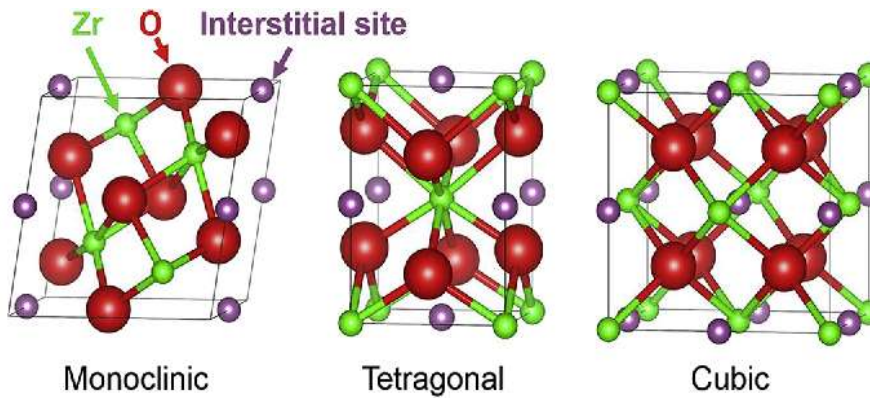


Figure 2.2. Crystallographic phases of ZrO_2 (Dong 2017)

The changes in the crystal structure of zirconia are reversible and are associated with changes in the volume and shape of the crystal cells. When cooling, there is a change in volume for the cubic to the tetragonal transition of around 2.5wt% and for the tetragonal-monoclinic phase transition of around 4wt%. Especially the $t \rightarrow m$ transformation that takes place at a temperature in the range of 1000–1200°C on cooling is of technological interest (Table 2.1).

Table 2.1. Physical properties of zirconia. (Piconi 2015)

Material	Zirconia		
	Monoclinic	Hexagonal	Cubic
Crystallography	Monoclinic	Hexagonal	Cubic
Lattice parameter a (nm)	0.5156	0.5094	0.5124
Lattice parameter b (nm)	0.5191	0.5177	-
Lattice parameter c (nm)	0.5304	-	-
Density (theoretical) (g/cm^3)	5.83	6.1	6.06
Melting point (K)	2790		
Thermal expansion coefficient	5-10		
Thermal conductivity (298K) (>99.9%TD) (W/mK)	2.5		

The deformation of the ZrO_2 polycrystal is due to both the expansion of the lattice and the shear force generated by the change in the shape of the tetragonal cell. This deformation, in turn, generates an increase in stress on neighboring untransformed grains. As a result, it can shatter sintered products of pure zirconium dioxide at a macroscopic level. Due to those facts, pure zirconia had found applicability as a refractory (for temperatures above 538°C) or as a pigment until around 1930, when

Ruff presented that at room temperature, zirconia stabilized to cubic phase (Ruff 1929). Due to its cost-effectiveness and highly effective index, it replaces diamonds in the jewelry industry.

Engineering applications of zirconia ceramics were made possible by discovering the stabilization of the tetragonal phase to room temperature. Garvie named the ceramic containing zirconia both in cubic and tetragonal phases, Partially Stabilized Zirconia (PSZ) due to the low concentration of the stabilizing oxide that determines the partial completion of the cubic phase (Garvie 1972). Initially, calcium oxide was used as a stabilizer to obtain PSZ, but later on, magnesium oxide (magnesia, MgO) or yttrium oxide (yttria, Y_2O_3) was used instead. Garvie and its team influenced the development of zirconia applications in 1975. They discovered that the transformation of the tetragonal phase into the monoclinic phase in Mg-PSZ led to an improved toughness (Garvie 1975). The best word to describe this transformation is "martensitic" because the transformation takes place due to mechanical deformation or when a temperature change occurs. The phase transition (i) is not associated with the transport of matter (it is diffusionless); (ii) is athermal because the transformation takes place between a range of temperatures instead of a specific one; and (iii) modifies the crystal lattice shape. Shortly after, Rieth (Rieth 1976) and Gupta (Gupta et al. 1978) showed successfully that a zirconia ceramic would be almost entirely formed by tetragonal grains at room temperature, by using yttrium oxide as a stabilizer of the tetragonal phase. These ceramic materials, called Ytria-Tetragonal Zirconia Polycrystal (Y-TZP), contained 2–3 mol% yttria. For Y-TZP, the predominant phase is the tetragonal one, with grains ranging between 300-500nm, presenting simultaneously minor phases such as cubic or monoclinic zirconia. It is noted that several oxides have been studied as stabilizers for zirconia (CaO, MgO, Y_2O_3 , CeO_2 , Er_2O_3 , Eu_2O_3 , Gd_2O_3 , Sc_2O_3 , La_2O_3 , and Yb_2O_3). In zirconia applied in biomedical applications, studies were focused on materials stabilized by CaO, MgO, and CeO. However, the ceramic that was developed industrially to produce medical devices was the one stabilized by Y_2O_3 (Lughi 2010).

The tetragonal grains can transform into monoclinic; the transformation implies some 4 % volume expansion in free grains, being the origin of the toughness of the material, e.g., of its ability to dissipate fracture energy. Due to the relieving pressure on the grain, when the crack is expanding in the material, the grains in the surrounding change into a monoclinic phase as an effect of the fracture. The neighboring grains then experience some strain to accommodate both the change in volume of the

transformed grain and the shear strain due to the change in the shape of the crystal cells.

These microstructural changes occur at the expense of the elastic stresses that lead to the advancement of the crack. At a macroscopic level, this increases the toughness of the material. It was observed that in addition to the dissipated energy described in the transformation phase, the fracture, in order to propagate in the material, must take into consideration the compressive stress field as a result of the volume expansion of the grains.

In order to explain how the transformation toughening mechanism takes place in zirconia ceramics, scientists like Lange, Becher, Hannink, and their teams provided different models (Lange 1982, Becher 1994 and Hannink 2000).

Briefly, the model proposed by (Lange 1982) explains the transformation in terms of change in total free energy (ΔG_{t-m}). This model describes the change in free energy as the sum of three quantities: (i) change in chemical-free energy (ΔG_c), (ii) strain energy as a result of transformed particles expansion (ΔG_{SE}), and (iii) variation in surface energy related to how the particle modifies its shape and to microcracking, e.g.

$$\Delta G_{t-m} = \Delta G_c + \Delta G_{SE} + \Delta G_s$$

It is a function of temperature, and chemical composition, the variation of strain energy ΔG_{SE} (>0) is a function of the matrix stiffness and residual stress as a processing effect, a fact that cannot be ignored in the case of a sintered polycrystal, because the thermal expansion coefficient of two different phases is not the same.

Finally, the third term (ΔG_s) is a variation of free energy related to grains surface modification in phase transition and the new surface formation related to microcracking.

As observed by Lughì and Sergio (Lughì and Sergio 2010), the effect of free energy change makes a difference at a grain size of about 10nm because we must consider the square shape of the crystal instead of the cube. To conclude, both the dissipated energy during transformation and the phase transformation effect on mechanical properties are related to the following characteristics of the material:

- the concentration of the stabilizer,
- the effect of matrix limitation over the grains,
- the grain size and shape, and the homogeneous distribution.

A balance between the characteristics mentioned above is needed to preserve the metastable state in Y-TZP, and it will improve the effect of transformation on materials' mechanical properties. The grains should be distributed homogeneously and must have a small size to elude the high energy necessary for transformation and decrease grain boundaries' size. The calibration of the stabilizer is of great importance to increase the tetragonal phase fraction contained at room temperature. Residual stresses in the matrix upon cooling due to differences in lattice shrinkage and the stiffness of the material also contribute to the energy barrier that occurs when the transformation from tetragonal to monoclinic takes place. Finally, care is to be given to maintain the structure of Y-TZP in a metastable state: it has been demonstrated by an experiment that there is a decrease in bending strength when the material is over-stabilized.

2.3. Zirconia Mechanical Properties

The mechanical properties of zirconia (Table 2.2) are thus justified by the transformation toughening mechanism.

Table 2.2. Mechanical properties of zirconia (Piconi 2015)

Property	Units	Y-TZP	Mg-PSZ
Density	g/cm ³	6	5.5
Average grain size	µm	0.3-0.5	40-70
Flexural strength	MPa	900-1200	400-650
Young modulus	GPa	210	210
Fracture toughness	MPa m ^{1/2}	7-9	8-11
Hardness	GPa	12.5	12.5

Since zirconia is an ionic ceramic polycrystal, the plastic strain before the break of metal and the metallic alloy is not the dissipative mechanism for fracture energy in this type of material.

Although zirconia has a high fracture strength, its toughness is lower than in metals, although twice the one of high-density alpha-alumina (9–12 MPa m^{1/2} vs. 4–6 MPa m^{1/2}). As a result, Y-TZP bending strength is above 900 MPa (4-point bending). The similarity between the elastic module of zirconia and titanium alloys is beneficial when designing metal to ceramic connections since microstrains under load are minimum.

The mechanical properties that make zirconia the perfect candidate for dentistry applications are hardness, thermal conductivity, toughness, and bending strength.

When grinding zirconia parts, the shallow value of thermal conductivity must be considered because progressive degradation of the mechanical properties of the material (Low-Temperature Degradation - LTD) might be caused by thermal spikes. It can also happen in total hip replacement bearing surfaces in case of starved lubrication when surface-to-surface contact will occur because the lubricating film is no longer present to support or protect the surfaces. This behavior, combined with zirconia's hardness (12-13 GPa) and sensitivity to scratching, does not recommend using zirconia in ceramic-ceramic Total Hip Replacement bearings.

To summarize, zirconia behaves differently depending on the concentration of the stabilizers, and it must be kept in mind its metastable aspect, a fact that influences both processing conditions and environmental conditions of zirconia parts when they are used in specific applications.

2.4. Zirconia Stability

It is already known that in Y-TZP ceramics, the transformation from tetragonal to monoclinic phase can happen instantly. Kobayashi and his team (Kobayashi 1981) discovered that a low temperature degradation (LTD) or hydrothermal transformation explains the different values of mechanical properties along with the transformation progress.

LTD is characterized by several well-assessed features: (i) the transformation progress begins at the material's surface and continues inside of the material; (ii) the transformation from monoclinic to tetragonal phase will have as effect a surface uplift; (iii) the stresses lead to grain pull-out and surface cracking; (iv) the transformation penetrates the material, enhancing the extent of the process; (v) as the cracks extension progresses, one can observe the decrease of the material density and the reduction in strength and toughness of the ceramic.

Piconi proved in his experiments that LTD could happen at room temperature and also in humid environments (Piconi 2016). However, it is enhanced at temperatures above 100°C under saturated steam.

Hydrothermal treatments of zirconia ceramics have been studied by Piconi (Piconi 1999) from the perspective of mechanical relevance in biomaterials. However, until now, no model can entirely explain this behavior (Lughi 2010).

The models more debated were proposed by (Sato 1985), (Yoshimura 1987), and more recently by (Chevalier 2009). According to the Sato model, as well as the Yoshimura model, the process starts with the local interaction of the water molecules with the preferential sites on the surface of the material. Thus, the Sato model shows the reaction of the Zr-O-Zr bridges at the border of the grains with water, generating Zr-OH type bonds (Sato 1985). The conditions for stabilizing the tetragonal phase at room temperature are also changed. This aspect, in turn, generates the transition to monoclinic and the succession of LTD events. Also, the Yoshimura model (Yoshimura 1987) considers the formation of Zr-OH bonds, which give origin to stress fields in the crystal lattice. Once higher than a given threshold, the transformation starts leading to material degradation with its progress. The model proposed by (Chevalier 2009) is based on the filling by O^{2-} ions of the oxygen vacancies due to the trivalent yttrium in the ZrO_2 lattice.

LTD is easily observable on Y-TZP but not for zirconia like (Mg-PSZ, Ce-TZP). In contrast, the mechanical behavior of these types of zirconia is surpassed mainly by the Y-TZP ones. This fact makes the latter ceramic the one preferred for clinical use, formerly in orthopedics and now in dentistry.

Specific parameters can influence and help in controlling the rate of strength degradation. These parameters are high density, homogenous distribution, uniform grain size, the small dimension of the grain, and proper tuning of yttria concentration. The manufacturing process will control all the parameters mentioned above, as well as the physical and chemical performance of the precursors. Then LTD is peculiar to each Y-TZP material and of each manufacturing process.

There are not many studies related to gadolinium doped zirconia. The partially or fully stabilized Gadolinium-containing zirconia materials have been prepared using mixed oxide solid-state, sol-gel, coprecipitation, and polymeric precursors (Ruff 1999, Garvie 1978, Garvie 1975). The selective synthesis of monodisperse pure-cubic Gd_3+ZrO_2 nanophase, with contents up to 40 mol% of Gd, has been recently reported using the hydrothermal method (Rieth 1976).

2.5. Zirconia Radioactivity

After 1985 due to the two catastrophic accidents at the nuclear power plants in Three Miles Island and Chernobyl, zirconia used in medical devices was also approached by its radioactivity. Zirconia ores are associated with ^{238}U , ^{232}Th , and their decay products in concentrations depending on the source. Therefore, the public health

authorities have started to monitor how radioactivity affects cost-effective zirconia with a low degree of purity used as refractory material (working at high temperatures). The production of the raw materials used to prepare the high-purity ceramic precursors of zirconia enacts the practical separation of radioactive contaminants from the powders. However, the use of zirconia in medical devices implies characterizing this feature. A significant number of studies were published during the first half of the 1990s during the standard ISO 13356 concerning zirconia for clinical implants (Piconi 1999) was introduced. Piconi has shown that during the purification of nuclear wastes, the separation technologies employed lead to chemicals useful for the manufacture of zirconia precursors with a high level of purity (Piconi 2000). These chemicals show a specific gamma activity <50 Bq/kg, specific to the human body (Piconi 2014). It has been observed that zirconia presents a lower specific activity compared to other bioceramics such as feldspathic porcelains used in dentistry.

Chapter 3

Materials and Methods

3.1. Hydrothermal synthesis

Considering the study of (Prakasam 2018), a comparison of the main synthesis routes for obtaining doped zirconia materials has been made. Based on this comparison, for the experimental part, it has been chosen the hydrothermal synthesis.

Table 3.1. Comparison of main synthesis routes as obtaining process for doped zirconia materials

Synthesis route	Solid-state process	Co-precipitation	Hydrothermal	Sol-gel	Spray pyrolysis
Composition control	Poor	Good	Excellent	Medium	Excellent
Morphology control	Poor	Medium	Good	Medium	Good
Particle size (nm)	>1000	>100	10-100	>10	>10
Hard agglomerates	Medium	High	Low	Medium	Low
Impurities (%)	0.5-1	Max. 0.5	Max. 0.5	0.1-0.5	0.1-0.5
Additional steps	Calcinations, milling	Calcinations, milling	No	Calcinations, milling	No
Scalability	Industrial	Industrial	<u>Demonstration</u>	<u>Demonstration</u>	R&D
Environmental impact	High	Moderate	Low	High	Moderate

The proposed method to obtain the materials is hydrothermal synthesis due to its efficiency regarding time, energy consumption, costs of materials, and eco-friendliness, but most of all due to the considerable amount of ceramic nanopowders obtained and its characteristics. For pure zirconia, the hydrothermal process is presented in figure 3.1.

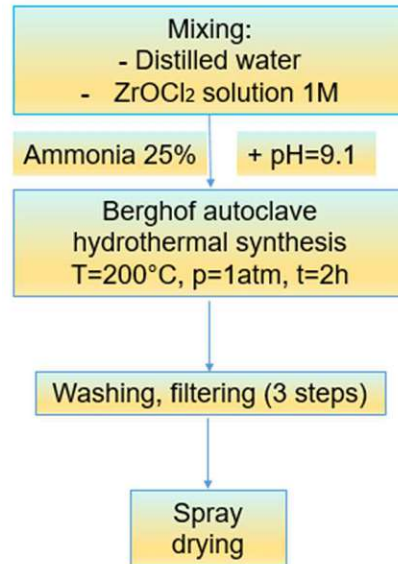


Figure 3.1. The hydrothermal flow for pure zirconia.

In the case of doped zirconia, figure 3.2 presents the process of hydrothermal synthesis.



Figure 3.2. Hydrothermal flow for doped zirconia.

The solutions were prepared to employ reactants purchased from Aldrich and used without a purification treatment in both cases. The solutions were mixed using a magnetic stirrer. Ammonia (25%) was the agent used to precipitate the solution and adjust the pH to 9.1. (Figure 3.3)



a)



b)



c)



d)

Figure 3.3. The doped zirconia solution precipitated in different stages (a to d)

The precipitate was transferred into a 5 l Teflon vessel in a Berghof stainless-steel autoclave, 80% filled, which was heated at 200°C for two h (see Figure 3.4).

The precipitates were then filtrated and washed three times with distilled water, then dried in an oven at 110°C for eight hours, as seen in Figures 3.5 and 3.6 in the case of doped zirconia, and then ground until a fine powder was obtained as in Figure 3.7, or dried using a spray drier in case of pure zirconia as in Figure 3.8.



a)



b)



c)

Figure 3.4. The Berghof autoclave (a to c)



a)



b)

Figure 3.5. The filtering process. (a and b)



a)



b)

Figure 3.6. The drying process in the oven for doped zirconia: a) before drying and b) after drying



Figure 3.7. Several stages of grinding

The significant advantage of spray drying (Fig 3.8) synthesized nanomaterials is the spherical shape of the grain, a fact that influence the porosity of the material, as will be discussed later in this work.



a)



b)



c)



d)



e)



f)

Figure 3.8. Spray drier system. (a to f)

- a) the clean set up device;
- b) detail of big vessel;
- c) detail of cyclone and collecting vessel at the beginning of spraying;
- d) subassembly of device;
- e) detail of cyclone and collecting vessel during spraying;
- f) the set up device during spraying

Pure ZrO_2 and RE doped zirconia were prepared using the same hydrothermal synthesis procedure, except for the drying procedure.

Finally, the prepared powders were calcined at $1400^\circ C$ for two hours. For each dopant (Y or Gd), having five wt% RE content - on an oxide basis, and for pure zirconia, samples were prepared for characterization.

3.2. Characterization methods

The obtained powders were characterized by morphology and phase composition, structure, and surface chemistry.

Each mentioned characterization method is further described in detail to understand the analysis better.

3.2.1. Scanning Electron Microscopy – SEM

The physical principles of electron microscopy

A cross-section through a modern electron microscope reveals the following constructive elements: the electro-optical column, the vacuum system, the systems for detecting, processing, and reproducing information, and the power supply block for all the components. The electro-optical column consists of the electron gun, condensing, and objective lenses.

The construction of an electron microscope is similar to the construction of the typical optical projector. The main parts common to the two instruments are the following: source (illumination - under an optical microscope, electrons - under an electron microscope), condenser lens (or condenser), sample to be analyzed, projector lens, and the system to visualize and record the information.

The role of the capacitor is to focus the electron beam on the sample, ensuring the best possible parallelism of the radiation with the optical axis. The lens forms the primary, magnified image of the object; this is taken over by the projector lens, magnifying it further for observation on the instrument screen.

The role of the electron cannon is to generate the electron beam. Inside the electron cannon, an electrostatic field directs the electrons emitted by a tiny portion of the surface of a filament through a very narrow aperture. After that, the cannon accelerates the electrons through the column directing them to the sample, with energies ranging from tens to tens of thousands of electron volts.

The electron beam emitted by the electronic cannon, which bombs the sample's surface, comprises monokinetic electrons called the incident or primary beam. Depending on the microscope used, it can be subjected to an acceleration voltage of 100V to 40,000V.

Several electron guns are currently used: tungsten, lanthanum hexaboride (LaB6), and field emission. Different materials and physical principles are used to obtain electron guns. Still, their common goal is to generate a directed electron beam with a stable current and a diameter as small as possible. The electron's trajectory inside the cannon is like a divergent beam. A series of electromagnetic lenses and diaphragms in the column reconverge and focus the beam into a reduced or smaller image. Near the bottom of the column are a few scanning coils in the raster, which deflect the electron beam in a scanning grid on the sample's surface. The final lens focuses the beam into an area as small as possible on the sample's surface.

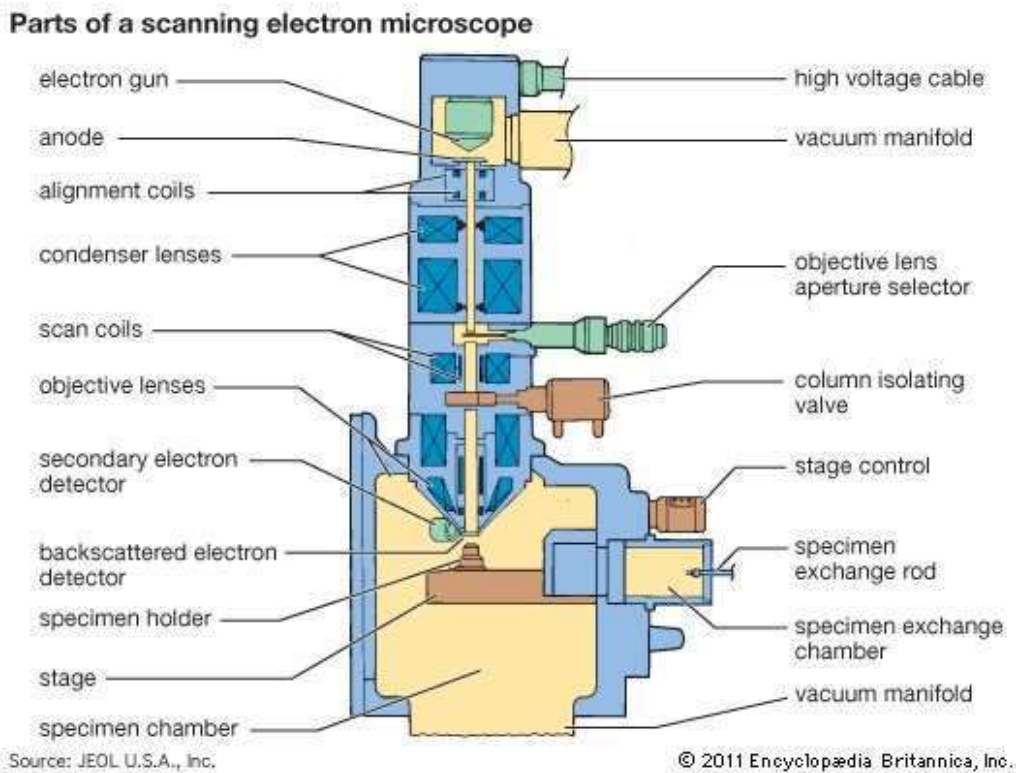


Figure 3.9. Schematic representation for a scanning electron microscope
(Source JEOL U.S.A., Inc. © Encyclopedia Britannica, Inc.)

After traversing the electron column, the beam reaches the test/sample chamber. It incorporates the sample handling device, a door for inserting or removing the

analyzed sample, and several devices for mounting signal detectors or other accessories. When the electron beam interacts with the sample's surface, several signals are produced. After being detected, amplified, and processed, it allows for obtaining information on the samples' morphology, structure, and composition.

As a result of interaction between the sample and the primary beam, the signals that can be observed are secondary electrons, backscattered electrons, Auger electrons, transmitted electrons (only for thin film samples), X-rays, cathodoluminescence, and induced electromotive voltage.

The size of the obtained signals depends on three factors: the thickness of the investigated sample, its chemical composition, and the acceleration voltage of the electrons.

In scanning electron microscopy, the principle of which has been stated above, incident electron beams with energies of 1-50 keV are used, which are either partially scattered backward (backscattered by elastic reflection on the sample atoms) or determine the emission of secondary electrons by interaction with the sample. Scattered electrons and secondary electrons are used for imaging in the scanning electron microscope.

In conventional transmission electron microscopy, the information is obtained employing electrons transmitted, not deflected, or scattered before, in the diaphragm of a lens that will form the electron microscopic image. In this case, the energies of the incident beam electrons are between 40 and 200 keV for conventional microscopes and between 200 keV and 3 MeV for high voltage electron microscopes. The scattering of electrons can be elastic (without significant energy losses and with a change of direction) or inelastic (with energy losses in which energy can be transferred to the sample or sample atoms in various ways). In the case of inelastic scattering, energy transfer can cause the excitation or ionization of bound electrons, either the excitation of free electrons or lattice vibrations (phonic vibrations) or the heating of the sample, or the irradiation defects formation. Measuring these energy losses can provide information on the chemical nature of the sample.

Another classification of electron scattering considers the number of scattering events involved: single and multiple scattering. In the first case, the electron undergoes a single interaction, a fact observed, for example, in the thin layers or foils studied in the transmission electron microscope. On the other hand, multiple scattering leads to a diffusive scattering in which the movement of electrons becomes random. This type of scattering is characteristic of the massive, thick samples studied in scanning electron microscopy.

The X-ray emission occurring at the sample impact with the electron beam, when analyzed with spectrometers, enhances the identification and the constituent element concentration.

Technical principles of Scanning Electron Microscopy

For a simplified overview, the operation of a scanning electron microscope is based on several steps (see figure 3.10):

- formation and acceleration of an electron beam
- the electron beam is delimited and concentrated using metal diaphragms and condensing lenses;
- when using the objective (final) lens, the beam is focused on the surface of the sample;
- the interactions generated inside the bombarded sample generate signals that are identified and transformed into an image or data on the content or concentration of the elements in the sample.

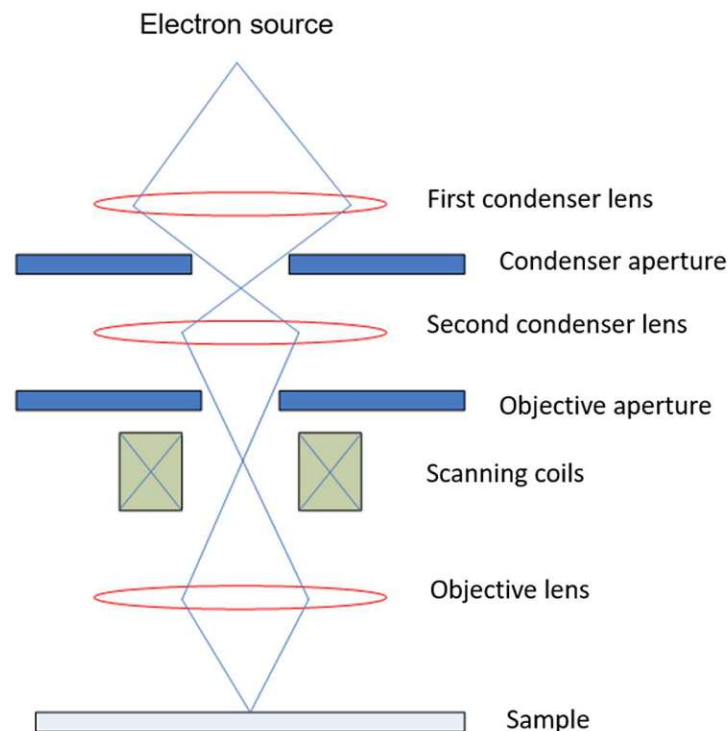


Figure 3.10. Schematic representation of how SEM is operated

© <https://www.unl.edu/ncmn-cfem/xzli/em/semoptic.htm>

3.2.2. Energy Dispersive X-ray analysis - EDX

This technique comprehensively maps the sample by analyzing near-surface elements and estimating the elemental proportion at different positions (Titus et al., 2019).

The EDX analysis and SEM work together and can be used simultaneously. When the conducting sample's surface is hit by an electron beam ranking between 10-20 keV, the material emits X-rays; thus, the material significantly influence the energy of the emitted X-rays.

Since the X-rays are generated in a region of around 2 μm in depth, the EDX is not considered a specific technique for surface science. However, moving the electron beam across the material can obtain an image of each element in the sample. Unfortunately, the required time to get an image is longer than 2 hours, a fact caused by the low intensity of the X-rays (Joshi et al., 2008).

EDX is a great tool that can estimate the amount of nanoparticles or composition at the surface or a few microns depth. They may contain some heavy metals ions. EDX can quickly identify/detect silver, gold, and palladium nanoparticles on the surface. However, for elements of low atomic number, EDX presents some difficulties in detecting them.

3.2.3. Fourier Transform Infrared spectroscopy (FTIR)

FTIR analysis uses infrared light to identify organic, inorganic, and polymeric materials by samples scanning. If the absorption band patterns show some changes, it points out a change in the material composition. FTIR is of great help in identifying and characterizing unknown materials. It can detect many contaminants in a material, detect additives, and identify oxidation and decomposition.

A schematic diagram of the FTIR spectrometer is depicted in figure 3.11. The main parts of a typical FTIR spectrometer are the source, sample cell, detector, amplifier, A/D convertor, and computer. Radiation from the source reaches the detector after it passes through the interferometer. First, the signal is amplified and converted to a digital signal by the A/D convertor and amplifier, being transferred to the computer. Then the Fourier transform is computed.

The infrared radiation of about $10,000 - 100 \text{ cm}^{-1}$ is sent through the sample. Only part of the radiation is absorbed, and the rest passes through. The sample converts the absorbed radiation to vibrational or rotational energy. The detected signal is a spectrum ranging from 4000 to 400 cm^{-1} , representing the sample's molecular fingerprint. Every molecule has a unique fingerprint, making FTIR an invaluable tool for chemical identification (Taha 2013).

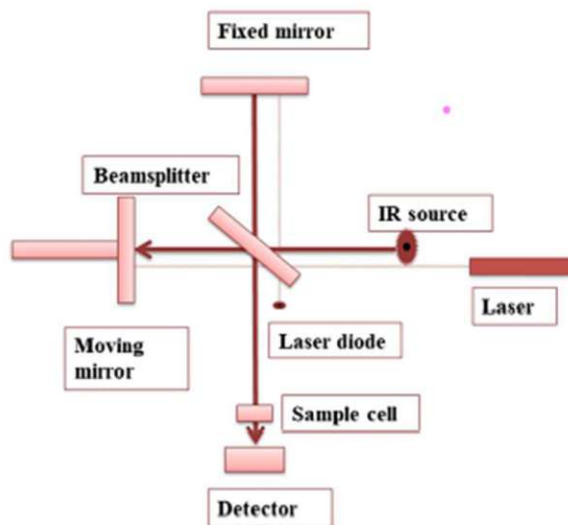


Figure 3.11. A schematic diagram of FTIR spectrometer (Titus et al. 2019)

3.2.4. X-ray Diffraction

The XRD analysis determines the crystallinity of the sample. Several additional information can be provided besides identification. XRD patterns can determine the element proportions if the sample is in mixture form. The data analysis is a factor that can influence not only the degree of crystallinity but any deviation of a particular element from its ideal composition and its structure. Only a part of the X-ray beam is transmitted at the interaction with the atomic planes. The rest of it is either absorbed or refracted, scattered and diffracted by the sample. X-rays are diffracted by each element differently, depending on the atomic arrangement and the type of atoms (Titus et al., 2019).

X-rays are shorter wavelength electromagnetic radiation, and they are produced at the deceleration of electrically charged particles with sufficient energy. A high voltage

is maintained between the electrodes, attracting electrons toward the metal target. At the impact point, X-rays are generated and radiate in every direction. These generated X-rays are collimated and directed to a finely ground powder sample. After the X-rays are detected, the signals are either processed with a microprocessor or done electronically. When the angle between the source, sample, and detector varies, it is obtained a spectrograph or a scan of the X-ray. Scattering occurs when the X-ray impinges a crystal lattice. Maximum scattering is eliminated as it interferes with itself, known as destructive interference. When the scattering comes in phase with the one from a different plane, diffraction occurs. Constructive interference occurs here as the reflections are combined to form new wavefronts (Titus et al., 2019). Each crystalline material has a distinctive atomic structure and diffracts the X-rays in a unique pattern. For measuring the angle of diffraction, Bragg's equation is used and is given by the following formula:

$$2d\sin\theta = n\lambda$$

Where: d - spacing between the planes

θ - the angle of incidence

n - an integer.

λ - the beam wavelength (Fig 3.12)

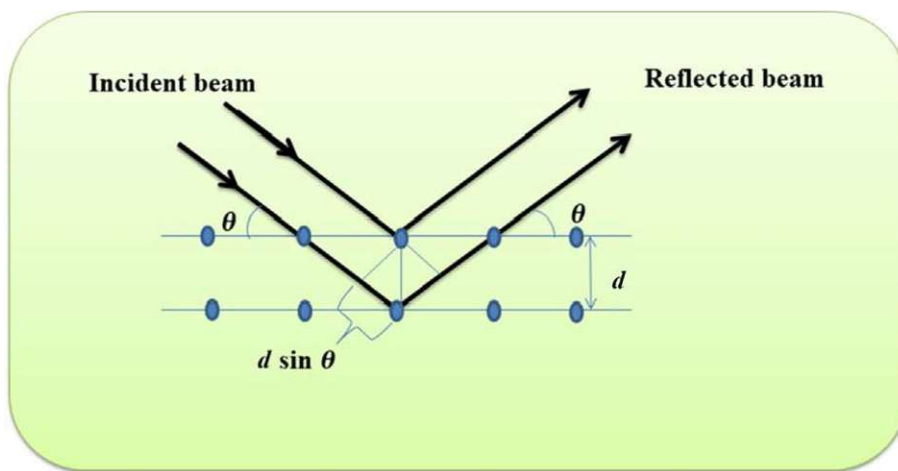


Figure 3.12. X-ray diffraction (Titus et al. 2019)

A simple graphic representation is shown in Figure 3.13. A radiation source and a detector for X-rays are located at the circumference of the graduated circle. The circle is centered on the powder specimen (Figure 3.13).

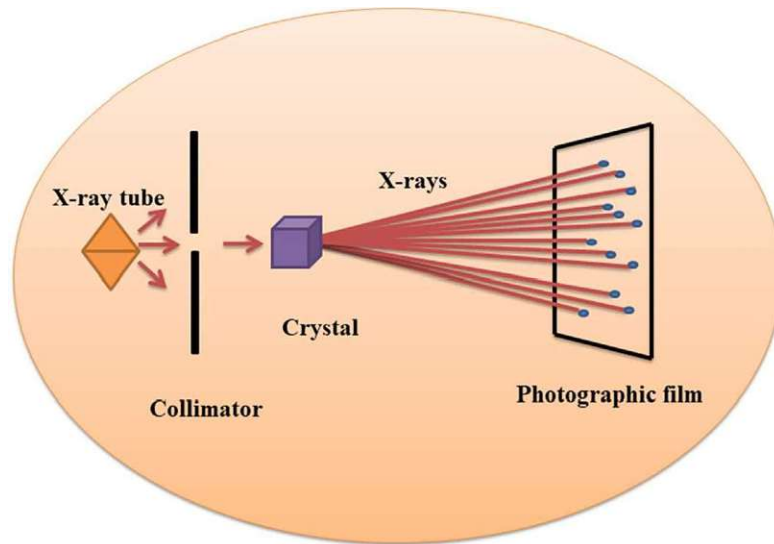


Figure 3.13. X-ray diffraction set-up (Titus et al. 2019)

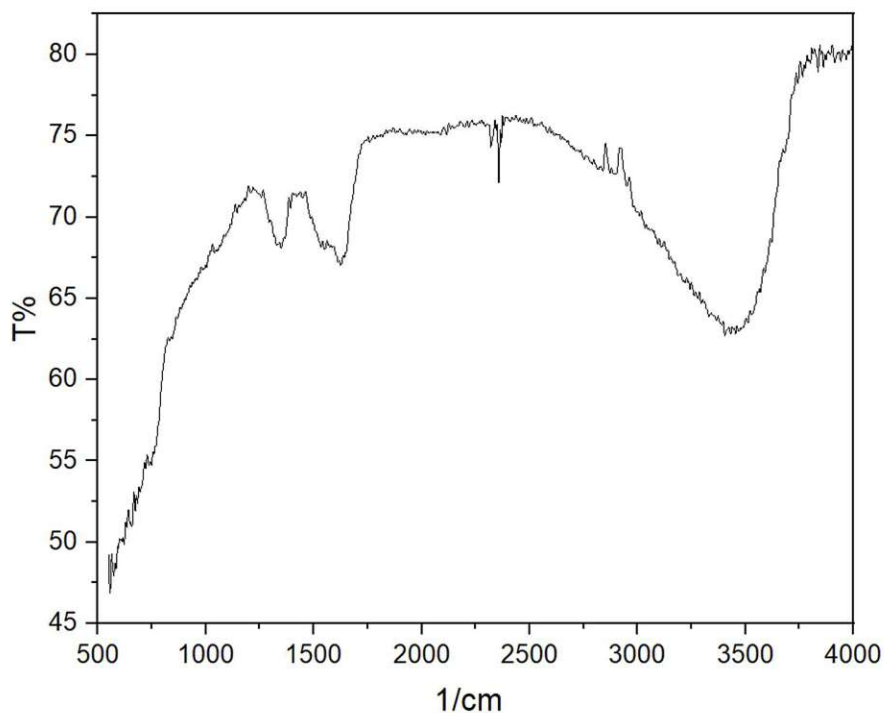
Divergent slits are situated between the specimen and the X-ray source and between the detector and the specimen. It helps limit the scattered radiation reducing the background noise, and the radiation is collimated. To get a ratio of 2:1 for the rotation of the sample simultaneously with that of the detector, the sample holder and detector are coupled to a goniometer.

Chapter 4

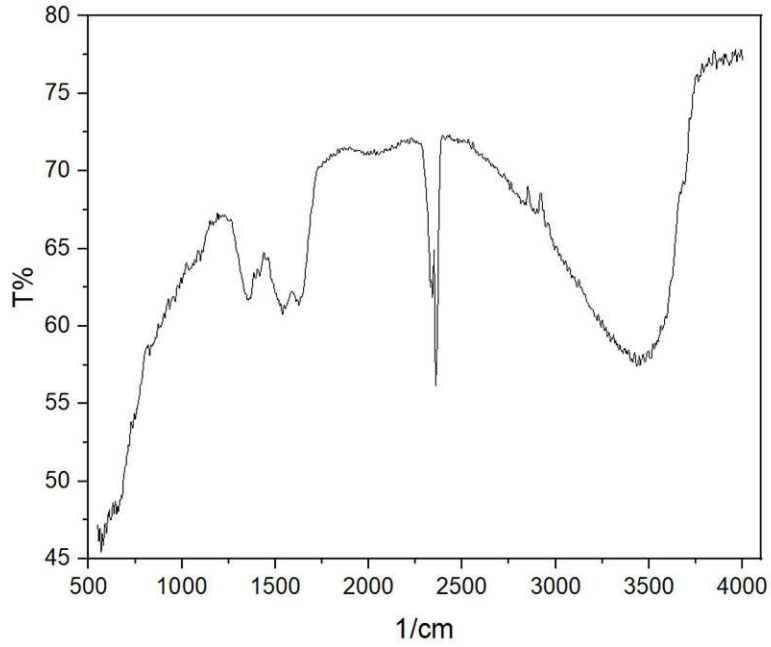
Results and discussions

4.1. FTIR analysis

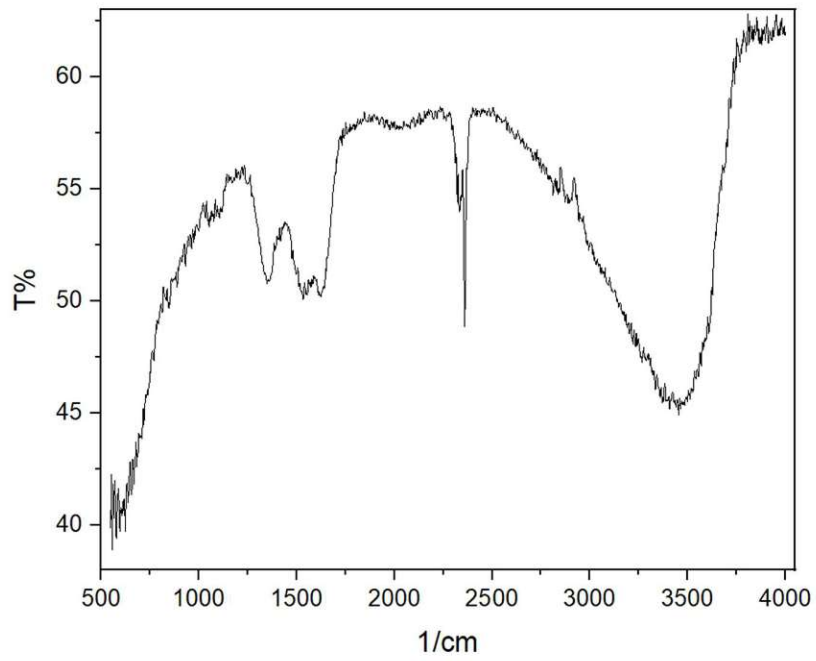
Fourier Transform Infrared spectroscopy (FTIR) was used to determine the chemical structure of the synthesized products in transmittance mode, the scanning range being from 550cm^{-1} to 4000cm^{-1} . First, KBr powder of one wt% concentration was added and mixed to the solid sample. The mixture thus obtained is milled for 20 minutes to grind grains and obtain fine, homogeneous particles. Eighty scans were done for data acquisition at an optical resolution of 4cm^{-1} .



a) Pure ZrO_2

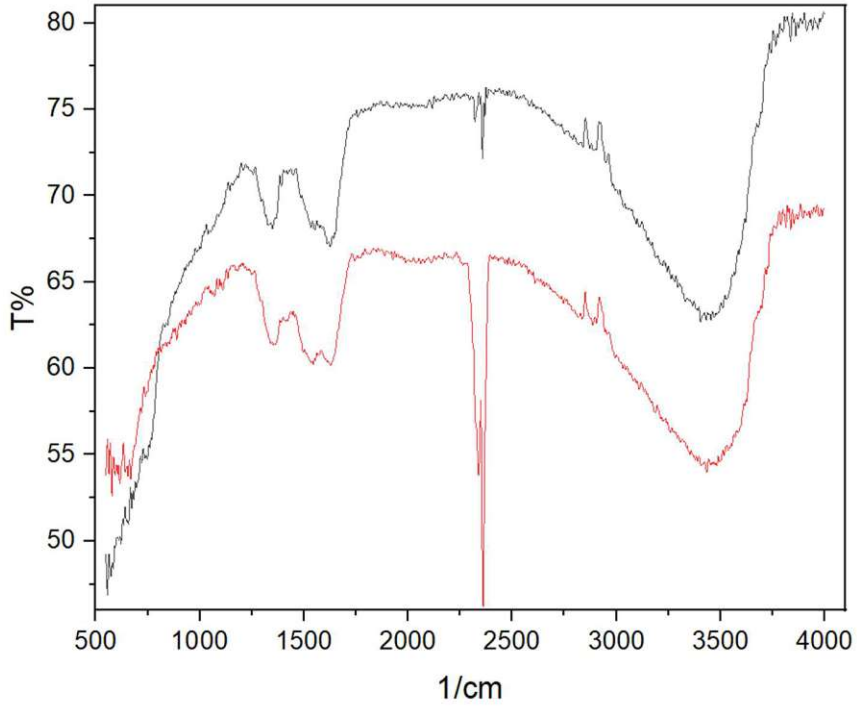


b) Y doped ZrO_2

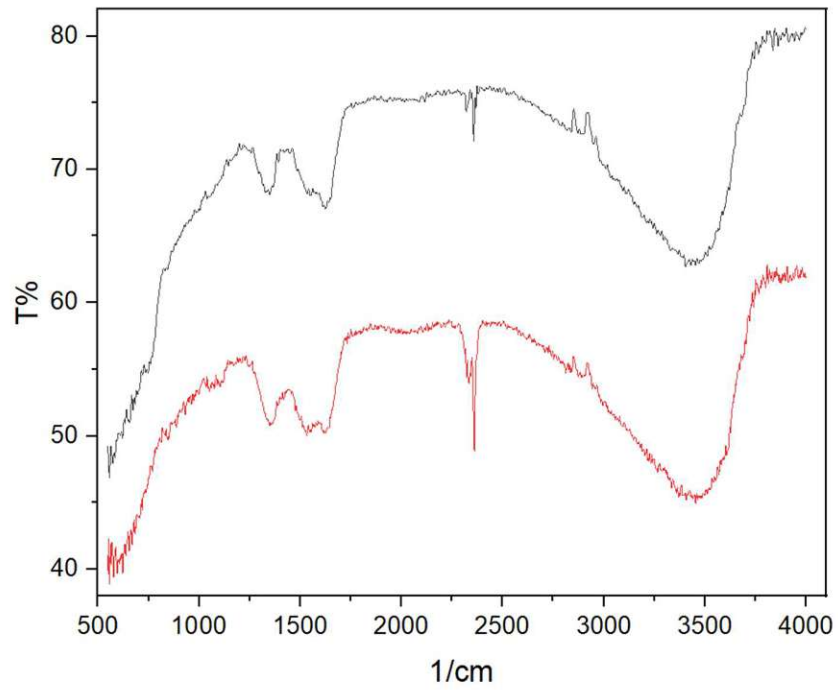


c) Gd doped ZrO_2

Figure 4.1. FTIR analysis for each sample:
a) pure ZrO_2 , b) Y doped ZrO_2 and c) Gd doped ZrO_2



a) Pure ZrO₂ compared with Y doped zirconia.



b) Pure ZrO₂ compared with Gd doped zirconia.

Figure 4.2. Overlaid spectra of a) Pure ZrO₂ compared with Y doped zirconia and b) Pure ZrO₂ compared with Gd doped zirconia.

Figures 4.1 and 4.2. present FTIR simple and overlaid spectra of the three samples: pure zirconia hydrothermally obtained powder and the rare-earth oxides (Y and Gd) doped zirconia.

In all samples, a sharp band is observed around 3600 cm^{-1} , specific to the stretching vibration of the hydroxyl group. A shoulder corresponding to the deformation band of the OH group (around $1630\text{-}1640\text{ cm}^{-1}$) is also observed, associated with the vibration from 3600 cm^{-1} . A massive band between $2350\text{-}2400\text{ cm}^{-1}$ is attributed to the asymmetrical stretching vibration of the CO_2 group. Vibrational bands attributed to the nitro (NO_3)- group (stretching vibration) can be observed at $1490\text{-}1540\text{ cm}^{-1}$. The shoulder from $1370\text{-}1375\text{ cm}^{-1}$ is also due to the nitro group. The peaks between $675\text{-}680\text{ cm}^{-1}$ could correspond to either halogen compounds (chlorides) or the metal-oxygen bond stretching vibration.

All peaks are better presented in table 4.1.

Table 4.1. Peaks registered during FTIR analysis.

Peak	Correspondence
3600 cm^{-1}	stretching vibration of hydroxyl (OH) group
$2350\text{ -}2400\text{ cm}^{-1}$	asymmetrical stretching vibration of CO_2 group
$1630\text{ - }1640$, shoulder cm^{-1}	shoulder of stretching vibration of hydroxyl (OH) group
$1490\text{-}1540\text{ cm}^{-1}$	stretching vibration of the nitro (NO_3) ⁻ group
$1370\text{-}1375$, shoulder cm^{-1}	shoulder of stretching vibration of the nitro (NO_3) ⁻
$675\text{-}680\text{ cm}^{-1}$	halogen compounds (chlorides) or the metal-oxygen bond stretching vibration

The sharp band associated with the stretching vibration of the hydroxyl group decreases considerably in intensity. The exact process is observed in the case of bands corresponding to the nitro group (probably due to the formation of secondary compounds). The decrease in peak intensity from $675\text{-}680\text{ cm}^{-1}$ could be explained by attributing this vibration to the Me-Cl group (formation of chlorides as reaction by-products).

4.2. XRD characterization

In order to examine the microstructure of the powders, it was used a device that can do qualitative analysis to identify crystalline phases in solids at a temperature ranging between 20–1500°C, as well as quantitative analysis of mixed powders, determining the crystallinity degree (based on Lorentz equation); diffraction domain ranges between $2\theta = 3\text{--}100^\circ$; maximum scanning rate 0,005 °/min.

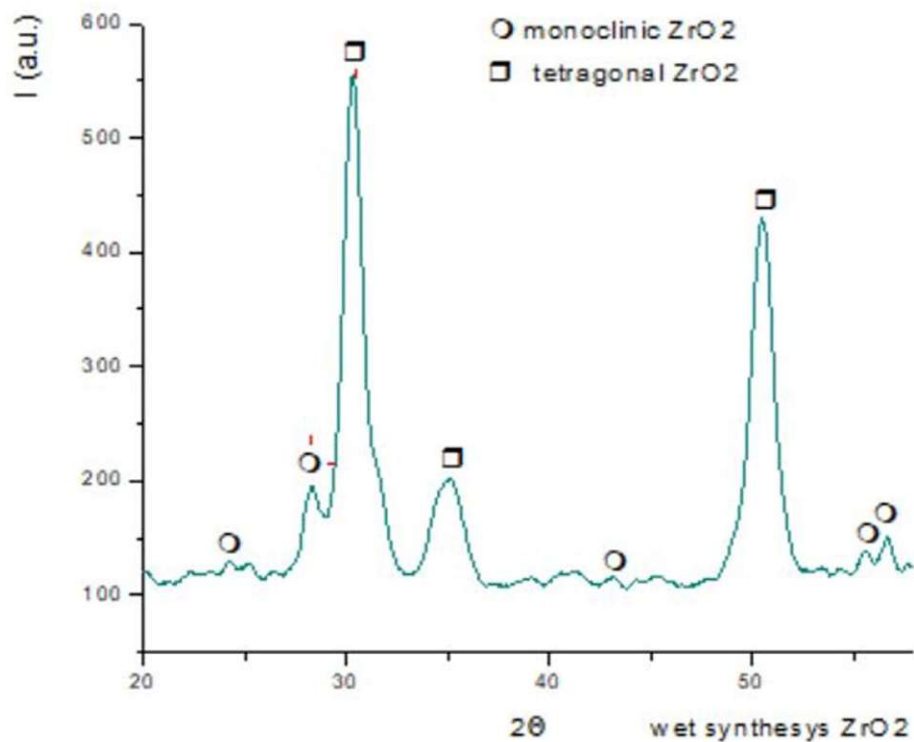
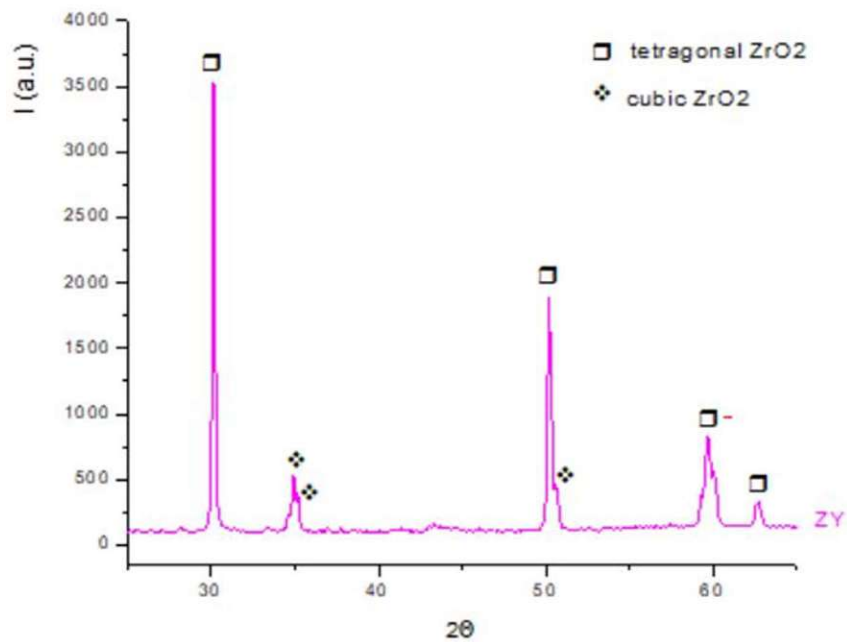
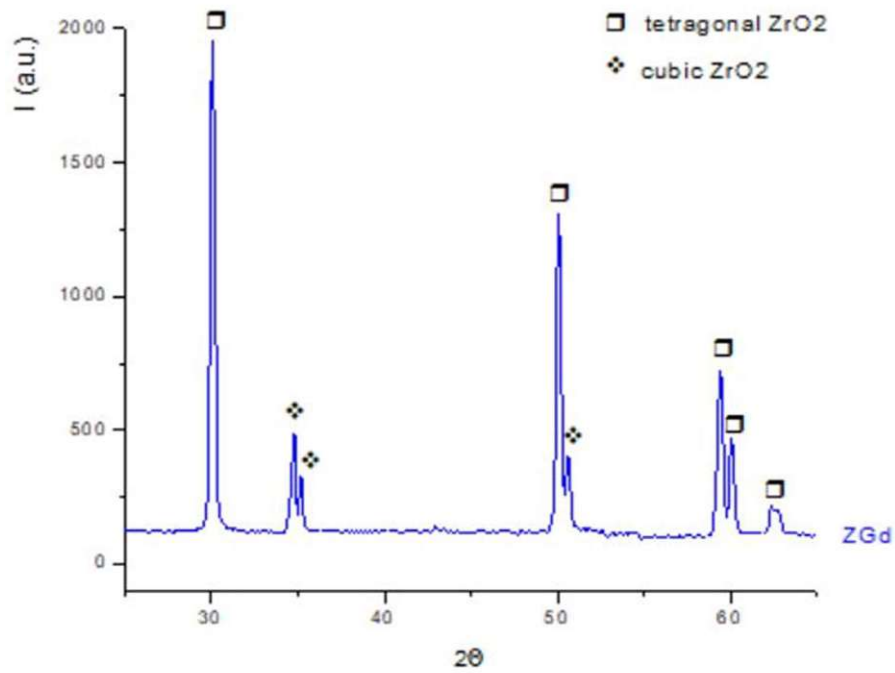


Figure 4.3. XRD for pure ZrO₂

The analyzed powder was spray dried. As can be seen from the XR diffraction spectrum, the powder contains more intense diffraction lines (diffraction peaks) specific to the ZrO₂ tetragonal phase mixed with lines of moderate monoclinic phase intensity - ZrO₂. The degree of crystallinity is low.



a)



b)

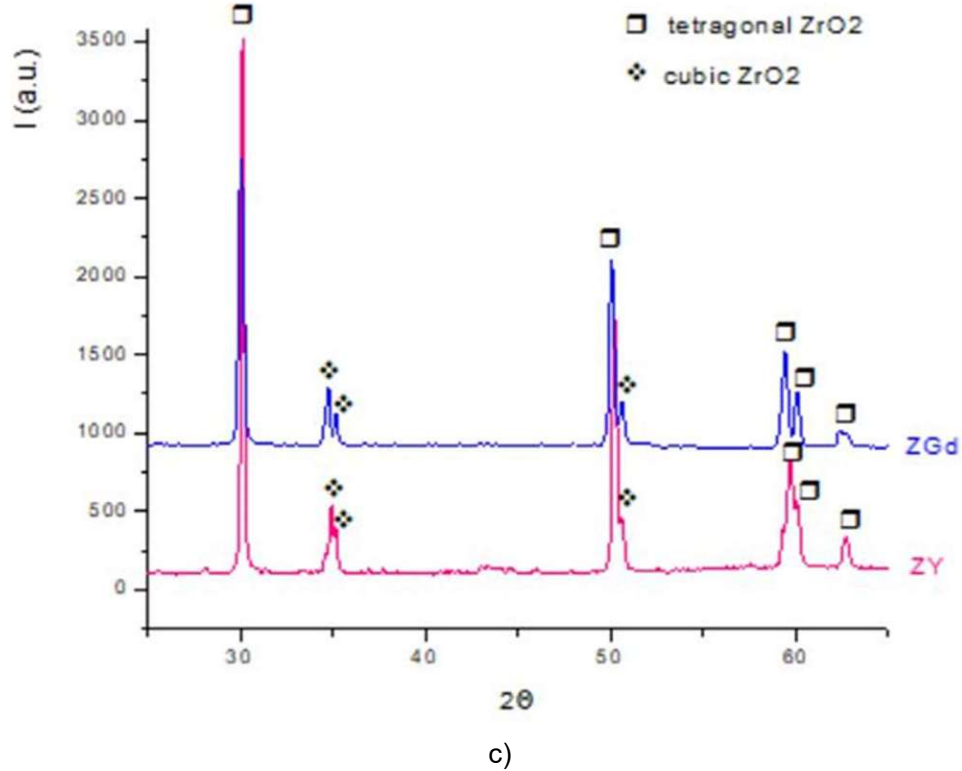


Figure 4.4. Diffraction image for calcined samples (Blue: $\text{ZrO}_2 + 5\% \text{Gd}_2\text{O}_3 - 1400^\circ\text{C}$, Purple: $\text{ZrO}_2 + 5\% \text{Y}_2\text{O}_3 - 1400^\circ\text{C}$) in simple form (a and b) and overlaid (c)

In both heat-treated samples, a reasonable degree of crystallinity is observed, which correlates with the microstructure of these samples (see scanning electron microscopy). In addition, samples with the two dopants presented a partial zirconia stabilization, obtaining a mixture of tetragonal and cubic phases- ZrO_2 .

It can be observed that there are no significant differences between the doped zirconia samples. Most of the peaks are in similar regions but with a different intensity.

For comparison reasons, figure 4.5 illustrates the findings of Leib (Leib et al., 2015). Zirconia and YSZ particles were synthesized in the presence of fatty acid stabilizers using an improved sol-gel method. The particles were heated up to 1500°C , but it can be observed that after heating to 1200°C , the particles were stable.

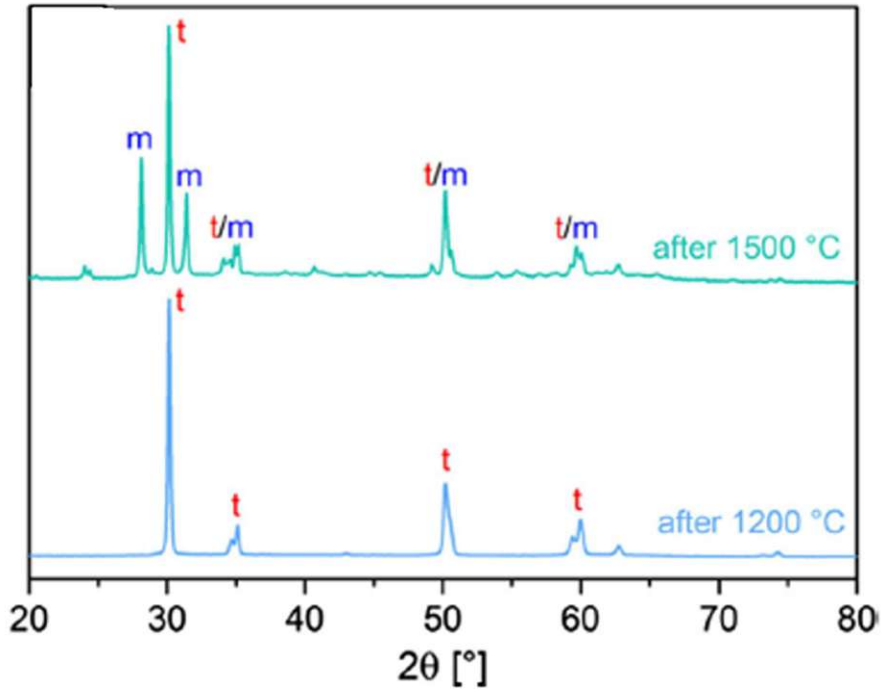
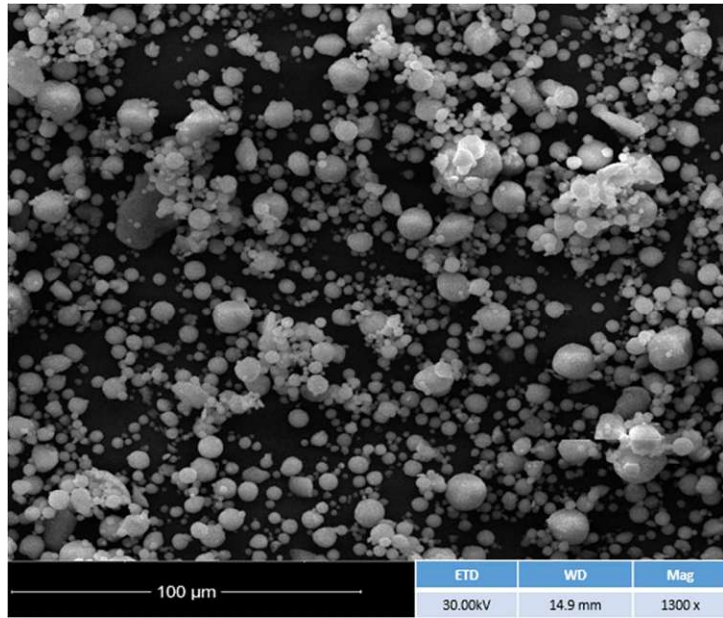


Figure 4.5. X-ray diffractograms for the yttria-stabilized particles after heating to 1200 °C and 1500 °C. (Leib et al., 2015)

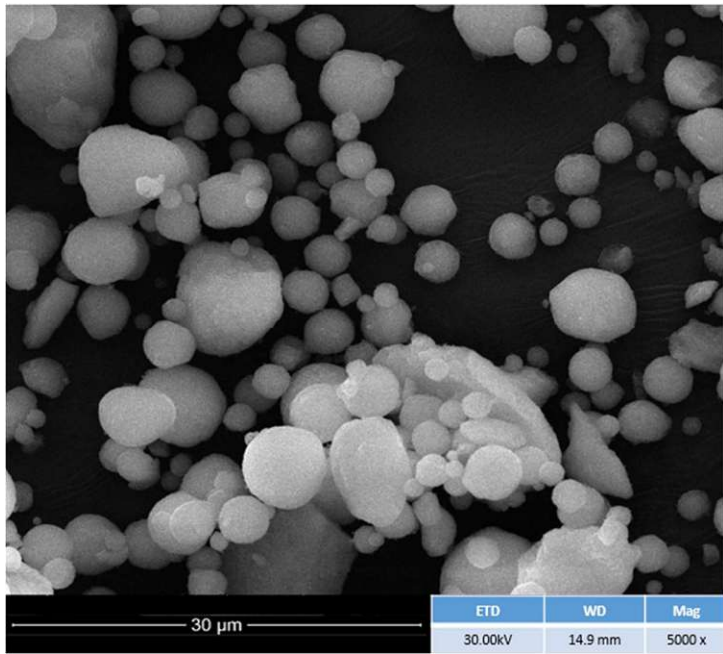
4.3. Scanning Electron Microscopy

A High-Resolution Scanning Electron Microscope was used for SEM analysis. The specifications are as follows:

- Ultrasensitive Directional Backscattered detector.
- High-resolution Schottky field emission (FEG)
- Accelerating voltage: 200 V to 30 kV
- Sample current: 200 nA



a)



b)

Figure 4.6. SEM analysis for pure zirconia sample

From the electron-microscopic images (Fig. 4.6. a-b), it can be seen that the powder has a spherical morphology, this being due to the processing method (hydrothermal synthesis) and more likely to the drying method. There is a tendency to agglomerate the powder due to the advanced fineness (nanometric dimensions).

For comparison reasons, Figure 4.7. presents the findings of Shi (Shi et al. 2012) for stabilized cubic zirconia nanoparticles fabricated via the vapor-phase hydrolysis process.

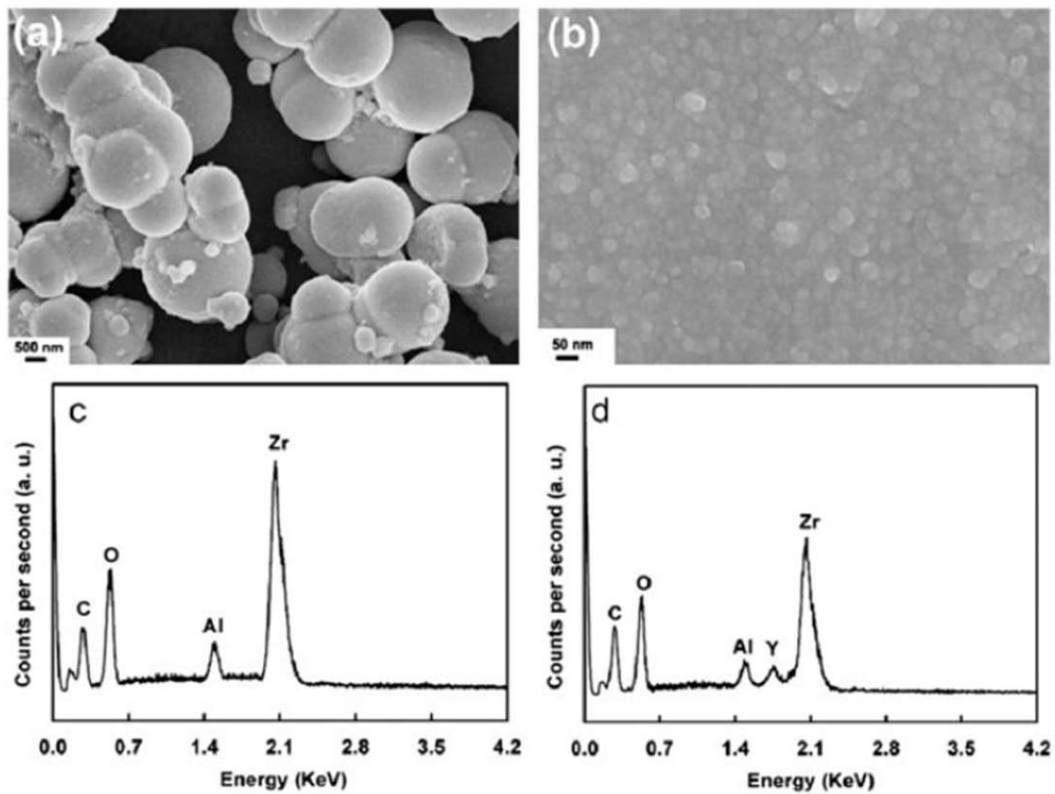
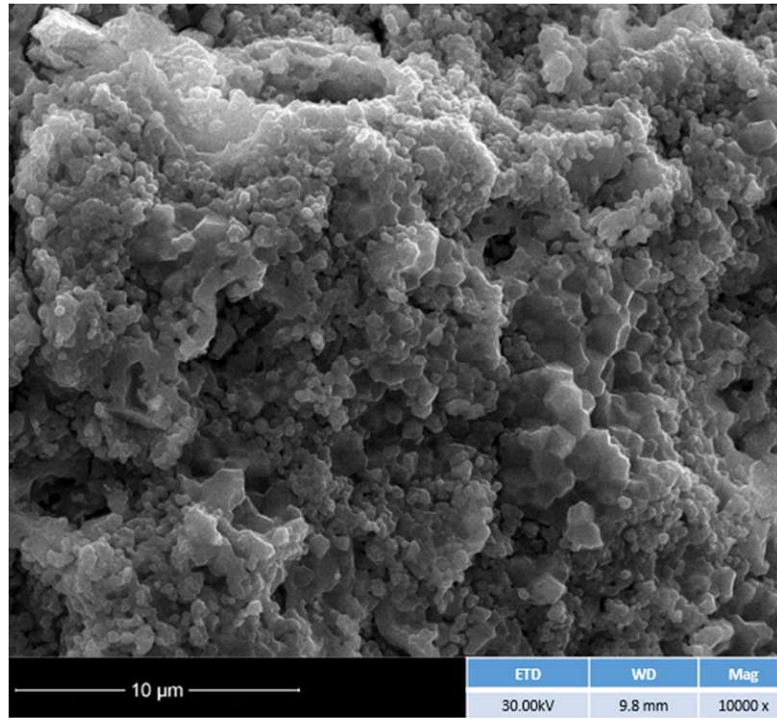


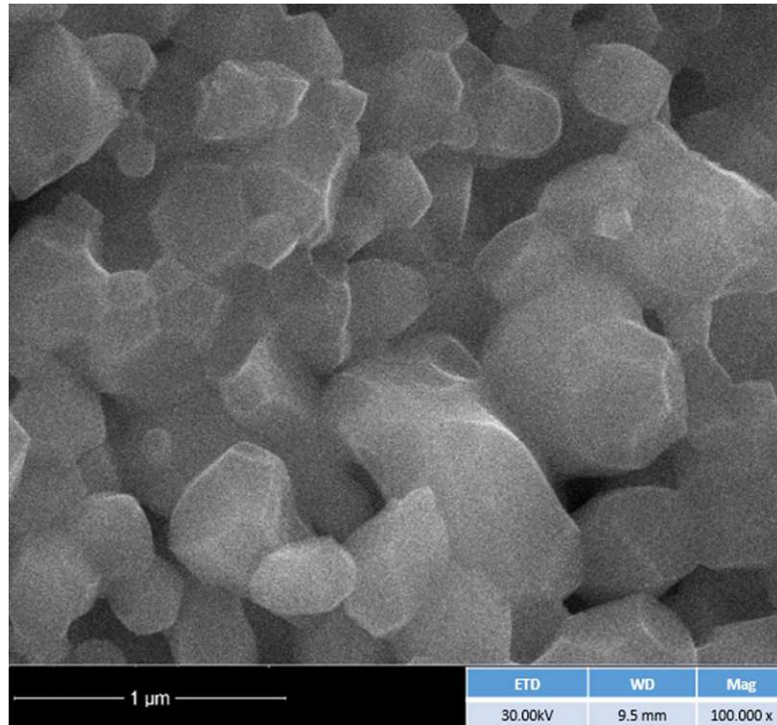
Fig. 4.7. SEM images of (a) pure ZrO_2 (0 mol%), (b) 8YSZ and EDX of (c) pure ZrO_2 (0 mol%), (d) 8YSZ. (Shi et al. 2012)

The analyzed powders were finely ground, pressed uniaxial at a pressing force of 100 MPa, in discs' shape, with a height of 5 mm and a diameter of 13 mm, and then heat-treated in a furnace at 5 °C / min, up to maximum firing temperature (1400 °C).

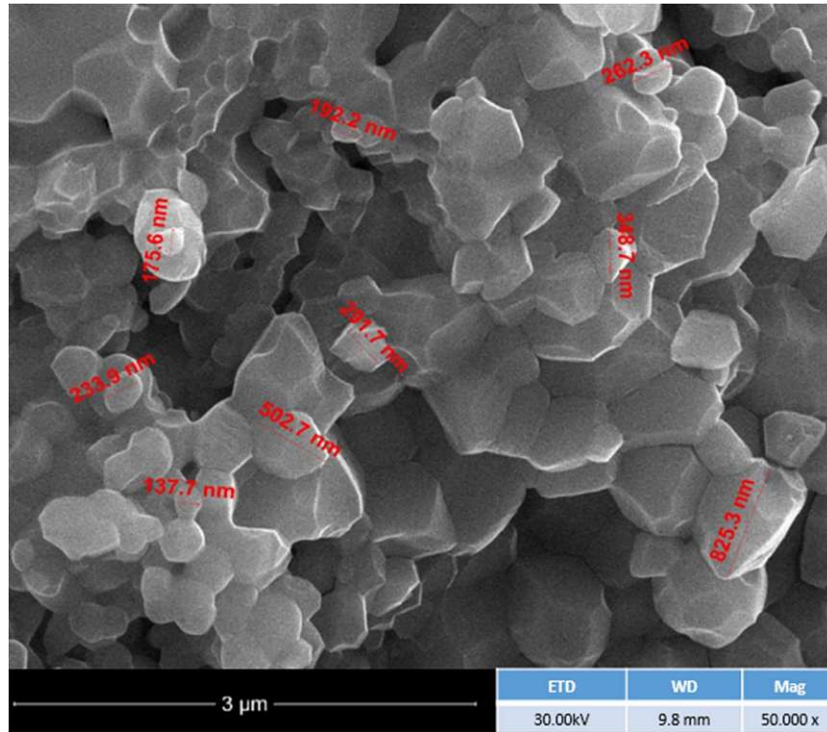
From the SEM analysis of the zirconia samples stabilized with yttrium at 1400 °C (Fig. 4.8 a-c), it is observed that the ceramic is well densified, showing well-defined granular limits polyhedral crystalline grains and an advanced degree of sintering.



a)



b)



c)

Figure 4.8. SEM analysis of the zirconia samples stabilized with yttrium at 1400 °C

In order to compare the results, SEM analysis from (Gosh et al., 2009) in Figure 4.9 and (Santos et al. 2019) in Figure 4.10 were used.

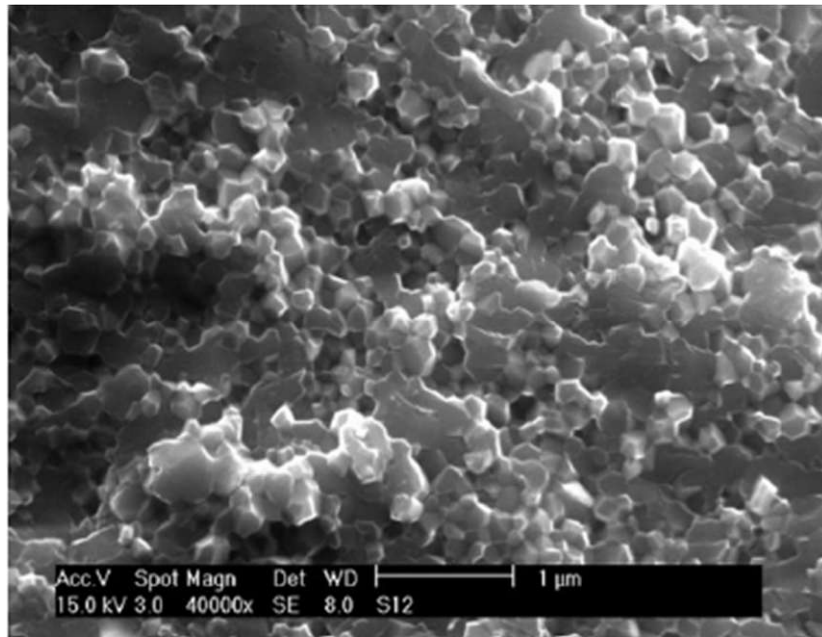
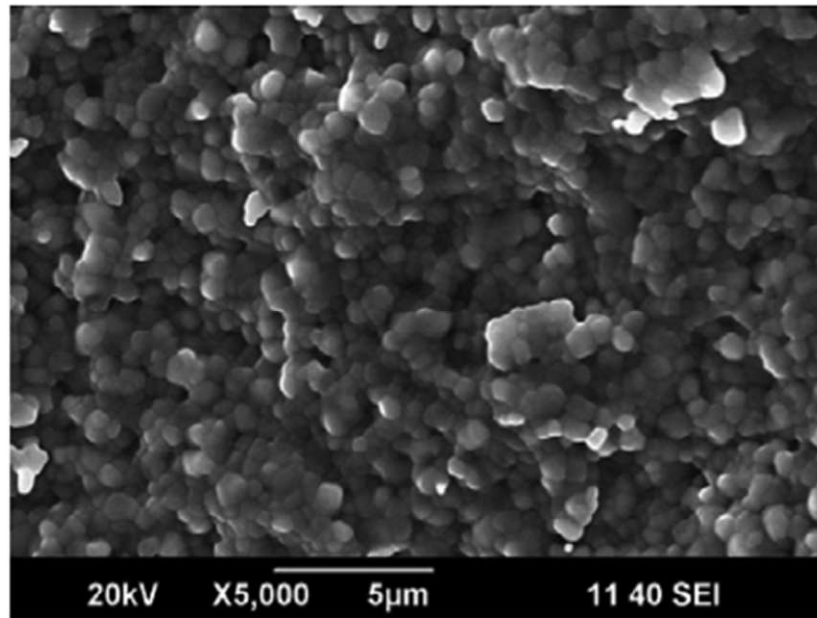
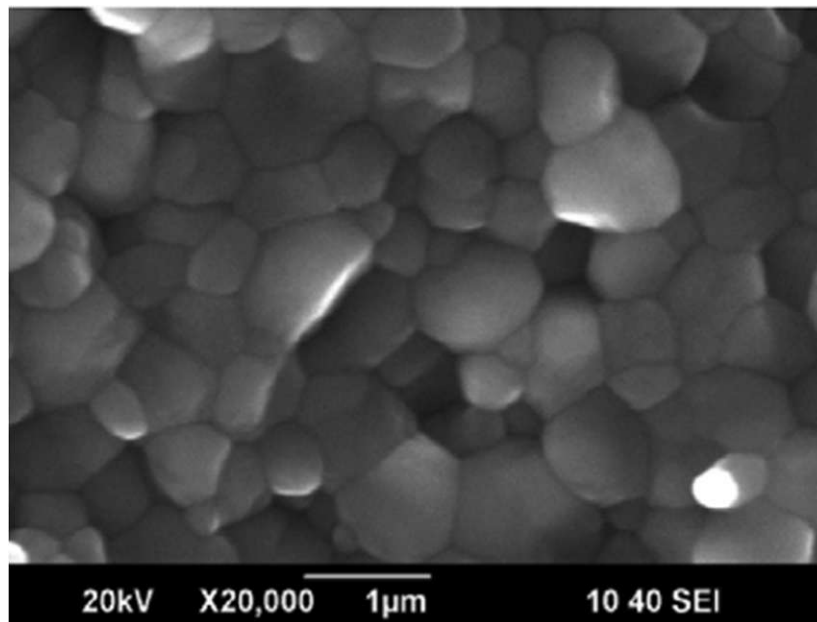


Figure 4.9. SEM analysis of a fracture surface of nanostructured YSZ (Gosh et al, 2009)



a)



b)

Figure 4.10. SEM micrograph of Y-TZP specimen sintered at 1530 °C for 2 hours.

(Santos et al. 2019)

In Figure 4.11, elemental compositions were confirmed by the energy dispersive X-ray (EDX) analysis.

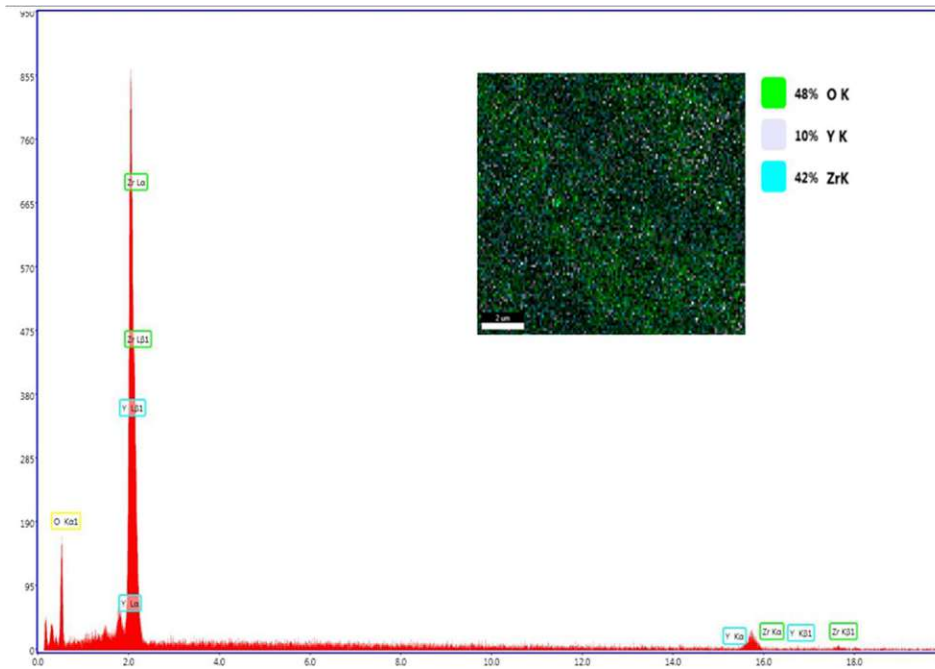
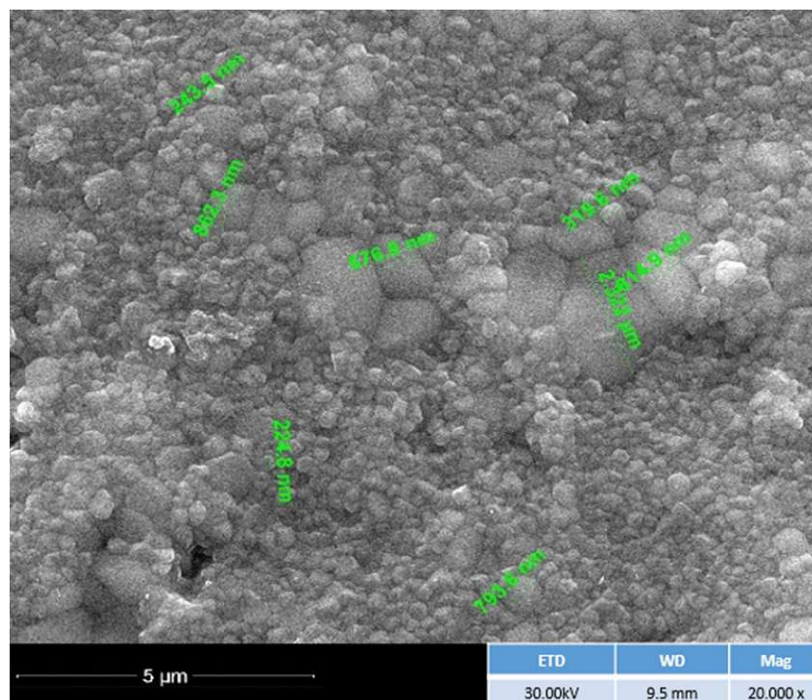
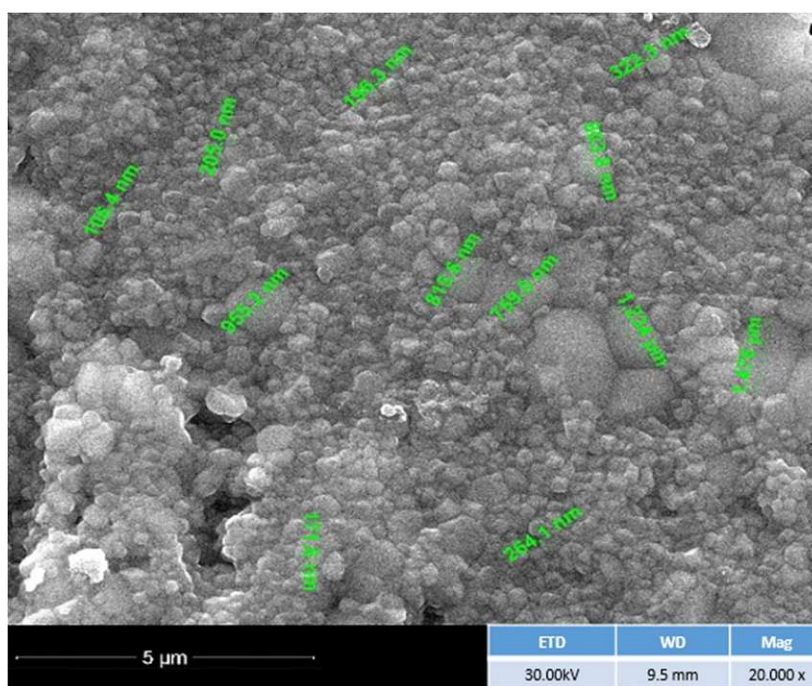


Figure 4.11. EDX analysis for Y doped zirconia

The powders processed by hydrothermal synthesis were heat-treated to sinter and stabilize the zirconia (seen in X-ray diffraction). As a result, the samples of Gd doped zirconia also show an intergranular microporosity (on the surface - Fig 4.12 a-b) and micron dimensions of the crystalline grains. However, in the section where the sample was broken (Fig 4.13 a-b), extremely good densification and size between 200nm to a few microns of crystalline grains are observed.

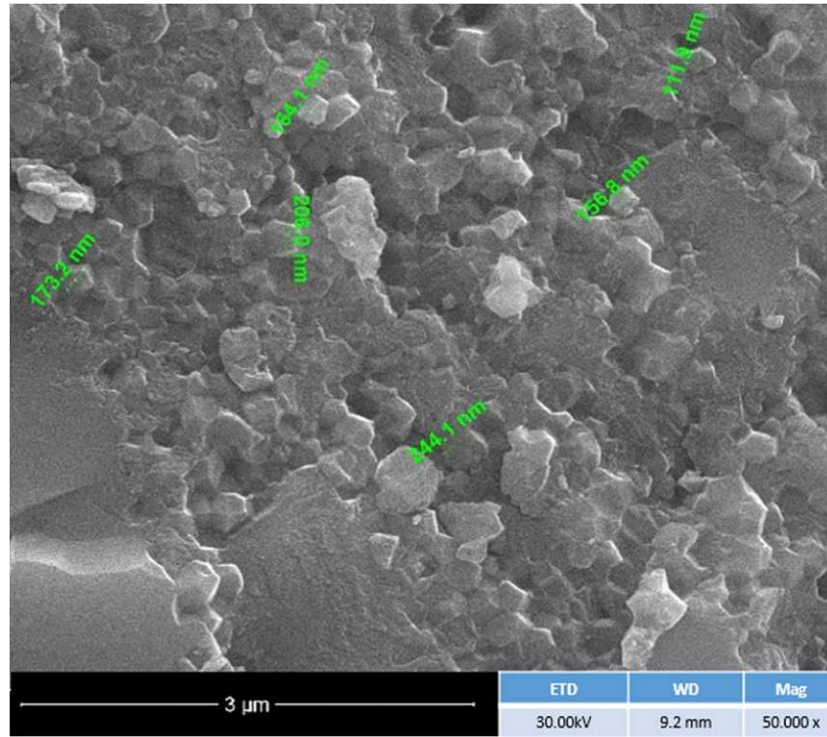


a)

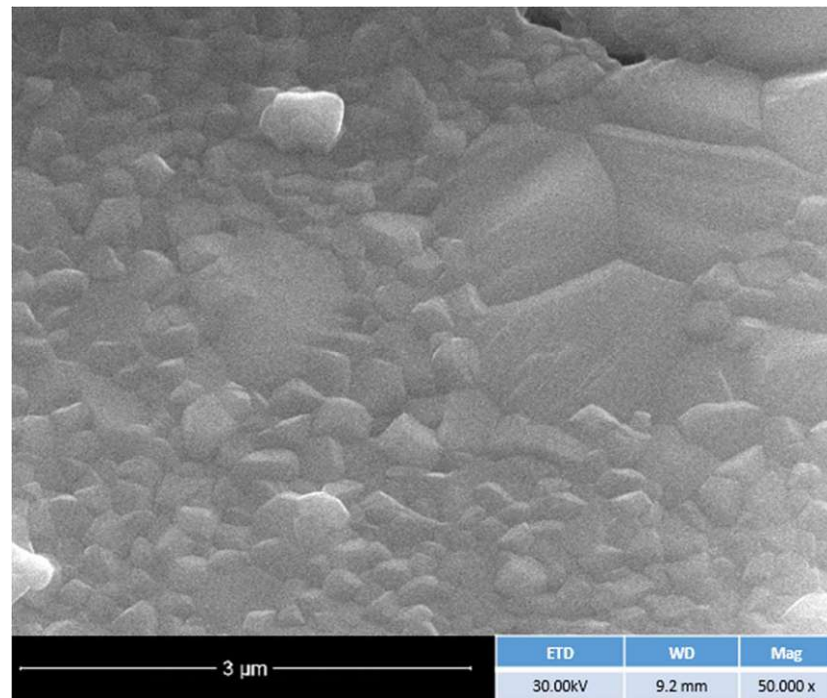


b)

Figure 4.12. a-b. SEM images for Gd doped zirconia



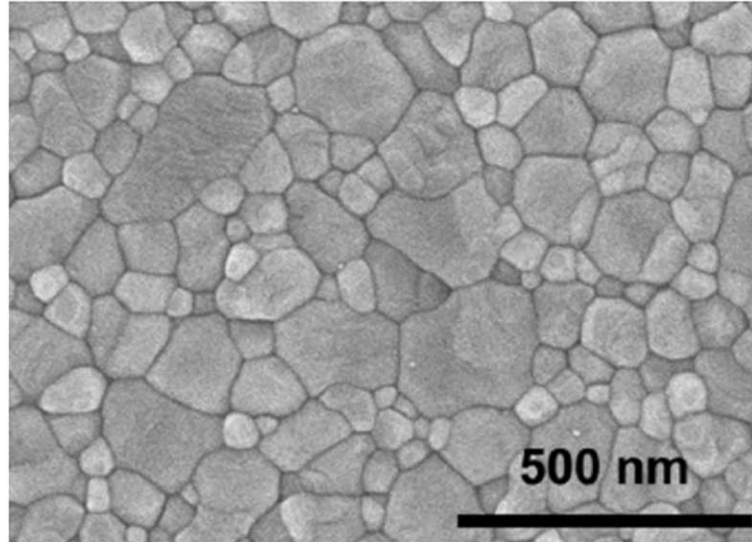
a)



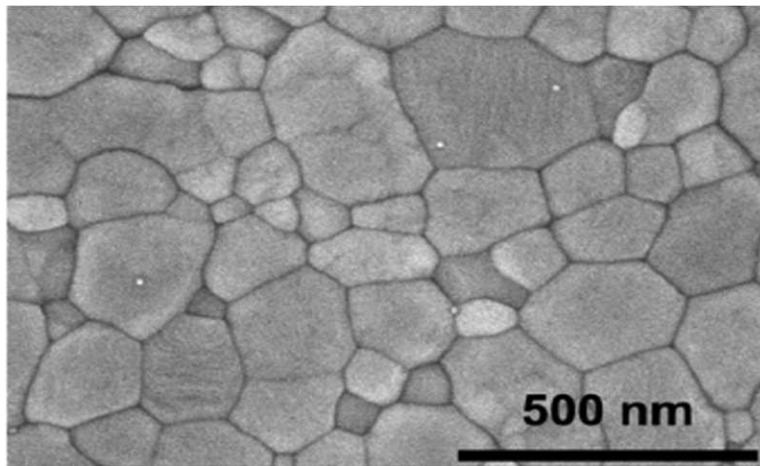
b)

Figure 4.13. a-b. SEM images for the breaking section of the Gd doped zirconia

For comparison reasons, (Merk, 2021) findings are presented in Figure 4.14. The powders were produced by mixing and milling pure zirconia powders and gadolinia oxide as a stabilizer and hot pressed in the 1250 °C – 1400 °C temperature range.



a) 1250 °C



b) 1400 °C

Figure. 4.14. Scanning electron microscopy images of thermally etched 3Gd-TZP based on M1 powder hot pressed at 1250–1400 °C (Merk, 2021)

Chapter 5

Conclusions

This thesis proposes to study three types of materials: pure zirconia, Y_2O_3 doped zirconia, and Gd_2O_3 doped zirconia as first-generation biomaterials. The hydrothermal method was chosen to synthesize the materials, and further specific characterization was carried out on the obtained samples.

The materials were analyzed by four characterization methods, considering the material's morphology, crystalline structure, and surface chemistry. Thus, Scanning Electron Microscopy and EDX, X-ray Diffraction, and Fourier Transform Infrared spectroscopy was performed.

As mentioned earlier, hydrothermal synthesis proved to be an excellent method to obtain ceramics because it provides reasonable control of the process and the repetitive behavior of materials regarding their properties, which can be observed further from the analysis described below.

SEM analysis revealed that pure zirconia tends to agglomerate the powder due to its advanced fineness (nanometric dimensions). In the case of using dopants like rare earth oxides of Y and Gd, the powders present a similar tendency to agglomerate, even though the dimensions of the particle are increasing from nanometric size to submicronic one. The heat treatment applied helped stabilize all the doped powders into a predominant tetragonal phase improving the densification degree as well. No conclusive differences between grains of ZrO_2 -Tetragonal and ZrO_2 -Cubic were observed in this work.

The XRD patterns obtained for the Y doped zirconia sample and the Gd doped zirconia samples are very similar. The XRD patterns show crystalline samples constituted by a mixture of two ZrO_2 polymorphs: tetragonal (t- ZrO_2) – the predominant and cubic (c- ZrO_2).

FTIR diagrams pointed out that, after thermal treatment, the sharp band attributed to the stretching vibration of the hydroxyl group decreases considerably in intensity.

The result of investigations demonstrates that medical applications of pure and RE doped zirconia are possible because it presents similarities compared to literature data of the similar studied materials.

However, further tests (such as in vitro) or mechanical properties characterization are needed better to understand materials' behavior or their biomaterial properties.

List of Abbreviations

REO – Rare Earth Oxide

XRD – X-Ray Diffraction

SEM – Scanning Electron Microscopy

FTIR – Fourier-Transform Infrared Spectroscopy

EDX – Energy Dispersive X-ray

Zirconia – Zirconium(II) oxide (ZrO_2)

Gadolinia – Gadolinium(III) oxide (Gd_2O_3)

Mg-PSZ – Magnesia - Partially Stabilized Zirconia

Y-TZP – Ytria-stabilized Tetragonal Zirconia Polycrystal

PSZ – Partially Stabilized Zirconia

LTD – Low-Temperature Degradation

Ce-TZP – Cerium-stabilized Tetragonal Zirconia Polycrystal

List of Figures

1	Figure 1.1. Interdisciplinary system of biomaterials	2
2	Figure 1.2: Biomaterials have made an enormous impact on the treatment of injury and disease and are used throughout the body	3
3	Figure 1.3: Primary requirements of new material design	4
4	Figure. 2.1. Microstructure of Y-TZP	9
5	Figure 2.2. Crystallographic phases of ZrO ₂	10
6	Figure 3.1. The hydrothermal flow for pure zirconia	18
7	Figure 3.2. Hydrothermal flow for doped zirconia	18
8	Figure 3.3. The doped zirconia solution precipitated in different stages (a to d)	19
9	Figure 3.4. The Berghof autoclave (a to c)	20
10	Figure 3.5. The filtering process (a and b)	21
11	Figure 3.6. The drying process in the oven for doped zirconia: a) before drying and b) after drying	21
12	Figure 3.7. Several stages of grinding	22
13	Figure 3.8. Spray drier system. (a to f)	23-25
14	Figure 3.9. Schematic representation for a scanning electron microscope	27
15	Figure 3.10. Schematic representation of how SEM is operate	27
16	Figure 3.11. A schematic diagram of FTIR spectrometer	31
17	Figure 3.12. X-ray diffraction	32
18	Figure 3.13. X-ray diffraction set-up	33
19	Figure 4.1. FTIR analysis for each sample: a) pure ZrO ₂ , b) Y doped ZrO ₂ and c) Gd doped ZrO ₂	34-35
20	Figure 4.2. Overlaid spectra of: a) Pure ZrO ₂ compared with Y doped zirconia and b) Pure ZrO ₂ compared with Gd doped zirconia	36
21	Figure 4.3. XRD for pure ZrO ₂	38

22	Figure 4.4. Diffraction image for calcined samples (Blue: $\text{ZrO}_2 + 5\%\text{Gd}_2\text{O}_3 - 1400^\circ\text{C}$, Purple: $\text{ZrO}_2 + 5\%\text{Y}_2\text{O}_3 - 1400^\circ\text{C}$) in simple form (a and b) and overlaid (c)	39-40
23	Figure 4.5. X-ray diffractograms for the yttria-stabilized particles after heating to 1200°C and 1500°C .	41
24	Figure 4.6. SEM analysis for pure zirconia sample	42
25	Figure 4.7. SEM images of (a) pure ZrO_2 (0 mol%), (b) 8YSCZ and EDX of (c) pure ZrO_2 (0 mol%), (d) 8YSCZ.	43
26	Figure 4.8. SEM analysis of the zirconia samples stabilized with yttrium at 1400°C	44-45
27	Figure 4.9. SEM analysis of a fracture surface of nanostructured YSZ	45
28	Figure 4.10. SEM micrograph of Y-TZP specimen sintered at 1530°C for 2 h.	46
29	Figure 4.11. EDX analysis for Y doped zirconia	47
30	Figure 4.12. a-b. SEM images for Gd doped zirconia	48
31	Figure 4.13. a-b. SEM images for the breaking section of the Gd doped zirconia	49
32	Figure. 4.14. Scanning electron microscopy images of thermally etched 3Gd-TZP based on M1 powder hot pressed at $1250\text{--}1400^\circ\text{C}$	50

List of Tables

1. Table 1.1: Applications of biomaterials.	4
2. Table 1.2: The brief classification of biomaterials based on their specific properties	6
3. Table 2.1: Physical properties of zirconia	10
4. Table 2.2: Mechanical properties of zirconia	13
5. Table 3.1: Comparison of main synthesis routes as obtaining process for doped zirconia materials	17
6. Table 4.1: Peaks registered during FTIR analysis	37

Bibliography

Becher PF, Francis Rose LR (1994) Toughening mechanisms in ceramic systems. In: Swain MV (ed) Structure and properties of ceramics, vol 11, Materials science and technology. VCH, Weinheim, pp 409–461

Cooke, F. W., Lemons, J. E., & Ratner, B. D. (1996). Chapter 1 — Properties of Materials. In B. D. Ratner, A. S. Hoffman, F. J. Schoen, & J. E. Lemons (Eds.), *Biomaterials Science* (pp. 11–35): Academic Press

Chevalier J, Gremillard L, Virkar AV, Clarke DR (2009) The tetragonal–monoclinic transformation in zirconia: lessons learned and future trends. *J Am Ceram Soc* 92:1901–1920

Dong, Y., Qi, L., Li, J., & Chen, I.-W. (2017). A computational study of yttria-stabilized zirconia: II. Cation diffusion. *Acta Materialia*, 126, 438–450. doi: 10.1016/j.actamat.2017.01.008

Fagelund, D., (1973) Determination of specific surface by the BET method, *Mat. Constr.*, 6, 239:245.

Garvie RC, Nicholson PS (1972) Structure and thermodynamical properties of partially stabilized zirconia in the CaO-ZrO₂ system. *J Am Ceram Soc* 55:152–157

Garvie RC, Hannink RHJ, Pascoe RT (1975) Ceramic steel? *Nature* 258:703–704

Ghasemi-Mobarakeh, L., Kolahreez, D., Ramakrishna, S., & Williams, D. (2019). Key terminology in biomaterials and biocompatibility. *Current Opinion in Biomedical Engineering*, 10, 45–50. doi: 10.1016/j.cobme.2019.02.004.

Ghosh, S., Teweldebrhan, D., Morales, J. R., Garay, J. E., & Balandin, A. A. (2009). Thermal properties of the optically transparent pore-free nanostructured yttria-stabilized zirconia. *Journal of Applied Physics*, 106(11), 113507. doi: 10.1063/1.3264613

Gul, H., Khan, M., & Khan, A. S. (2020). Chapter 3 — Bioceramics: Types and clinical applications. In A. S. Khan & A. A. Chaudhry (Eds.), *Handbook of Ionic Substituted Hydroxyapatites* (pp. 53–83): Woodhead Publishing.

Gupta TK, Bechtold JH, Kuznickie RC, Cadoff LH, Rossing BR (1978) Stabilization of tetragonal phase in polycrystalline zirconia. *J Mater Sci* 13:1464

Hannink RHJ, Kelly PM, Muddle BC (2000) Transformation toughening in zirconia-containing ceramics. *J Am Ceram Soc* 83:461–487

He, W., & Benson, R. (2017). Chapter 8 — Polymeric Biomaterials. In M. Kutz (Ed.), *Applied Plastics Engineering Handbook (Second Edition)* (pp. 145–164): William Andrew Publishing.

Joshi M, Bhattacharyya A. Ali S.W. (2008) Characterization techniques for nanotechnology applications in textiles, *Indian Journal of Fibre and Textile Research* ISSN 09710426, Volume 33, Issue 3, Pages 304 - 317

Kobayashi K, Kuwajima H, Masaki T (1981) Phase change and mechanical properties of ZrO_2 - Y_2O_3 solid electrolyte after aging. *Solid State Ion* 3–4:461–487

Kranthi Kiran A. S. K., Ramakrishna S., (2021) An Introduction to Biomaterials Science and Engineering – Chapter 4 Biomaterials: Basic principles, Pages: 412, <https://doi.org/10.1142/12038>

Kuhn, L. T. (2005). Chapter 6 — Biomaterials. In J. D. Enderle, S. M. Blanchard, & J. D. Bronzino (Eds.), *Introduction to Biomedical Engineering (Second Edition)* (pp. 255–312): Academic Press

Labani M.M., Rezaee R., Saeedi A., Hinai A.A., (2013), Evaluation of pore size spectrum of gas shale reservoirs using low pressure nitrogen adsorption, gas expansion and mercury porosimetry: a case study from the Perth and Canning Basins, Western Australia, *J. Pet. Sci. Eng.* 112, 7e16

Lange FF (1982) Transformation toughening – part 1–4. *J Mater Sci* 17:225–263

Leib, E. W., Vainio, U., Pasquarelli, R. M., Kus, J., Czaschke, C., Walter, N., ... Vossmeier, T. (2015). Synthesis and thermal stability of zirconia and yttria-stabilized zirconia microspheres. *Journal of Colloid and Interface Science*, 448, 582–592. doi: 10.1016/j.jcis.2015.02.049

Lughi V, Sergo V (2010) Low temperature degradation -aging- of zirconia: a critical review of the relevant aspects in dentistry. *Dent Mater* 26:807–820

Marin, E., Boschetto, F., & Pezzotti, G. (2020). Biomaterials and biocompatibility: A historical overview. *Journal of Biomedical Materials Research Part A*, 108(8), 1617–1633. doi: 10.1002/jbm.a.36930.

Merk, A.-L., & Kern, F. (2021). Influence of starting powder choice on structure property relations in gadolinia stabilized zirconia 3Gd-TZP manufactured from co-

milled starting powders. *Journal of the European Ceramic Society*, 41(15), 7783–7791. doi: 10.1016/j.jeurceramsoc.2021.08.002

Piconi C, Maccauro G (1999) Zirconia as a ceramic biomaterial. *Biomaterials* 20:1–25

Piconi C, Casarci M (2000) Purification of chemicals for the production of biomedical grade YTZP ceramics. In: Rammlair D, Mederer J, Oberthur RB, Petinghaus H (eds) *Applied mineralogy*. Balkema, Rotterdam, pp 205–207

Piconi C, Condò SG, Kosmac T (2014) Alumina- and zirconia-based ceramics for load bearing applications. In: Shen JZ, Kosmac T (eds) *Advanced ceramics for dentistry*, 1st edn. Butterworth-Heinemann, Waltham, pp 220–253

Piconi, C., & Porporati, A. A. (2015). Bioinert Ceramics: Zirconia and Alumina. *Handbook of Bioceramics and Biocomposites*, 1–25. doi: 10.1007/978-3-319-09230-0_4-1

Piconi, C., & Porporati, A. A. (2016). Bioinert Ceramics: Zirconia and Alumina. *Handbook of Bioceramics and Biocomposites*, 59–89. doi: 10.1007/978-3-319-12460-5_4

Prakasam, M., Valsan, S., Lu, Y., Balima, F., Lu, W., Piticescu, R., & Largeteau, A. (2018). Nanostructured Pure and Doped Zirconia: Synthesis and Sintering for SOFC and Optical Applications. *Sintering Technology - Method and Application*. doi:10.5772/intechopen.81323

Ramakrishna, S., Ramalingam, M., Kumar, T. S. S., & Soboyejo, W. O. (2010). *Biomaterials: A Nano Approach*: CRC Press Taylor & Francis.

Ratner, B. D. (1996). *Biomaterials Science: An interdisciplinary Endeavor*. In B. D. Ratner, A. S. Hoffman, F. J. Schoen, & J. E. Lemons (Eds.), *Biomaterials Science* (pp. 1–8): Academic Press.

Ratner, B. D., & Zhang, G. (2020). Chapter 1.1.2 — A History of Biomaterials. In W. R. Wagner, S. E. Sakiyama-Elbert, G. Zhang, & M. J. Yaszemski (Eds.), *Biomaterials Science (Fourth Edition)* (pp. 21–34): Academic Press.

Rieth PH, Reed JS, Naumann AW (1976) Fabrication and flexural strength of ultra-fine grained yttria stabilised zirconia. *Bull Am Ceram Soc* 55:717

Ruff O, Ebert F, Stephen E (1929) Contributions to the ceramics of highly refractory materials: II, System Zirconia-Lime. *Z Anorg Allg Chem* 180:215–224

- Santos, C. dos, Simba, B. G., Silva, R. R., Rodrigues Pais Alves, M. F., Magnago, R. O., & Elias, C. N. (2019). Influence of CAD-CAM milling on the flexural strength of Y-TZP dental ceramics. *Ceramics International*. doi: 10.1016/j.ceramint.2019.02.07
- Sato T, Shimada M (1985) Transformation of yttria-doped tetragonal ZrO₂ polycrystals by annealing in water. *J Am Ceram Soc* 68:356–359
- Shi, F., Li, Y., Wang, H., & Zhang, Q. (2012). Fabrication of well-dispersive yttrium-stabilized cubic zirconia nanoparticles via vapor phase hydrolysis. *Progress in Natural Science: Materials International*, 22(1), 15–20. doi: 10.1016/j.pnsc.2011.12.003
- Taha M, Hassan M, Essa S, Tartor Y. (2013) Use of Fourier transform infrared spectroscopy (FTIR) for rapid and accurate identification of yeasts isolated from human and animals. *Int J Vet Sci Med* 2013;1(1):15-20
- Titus, D., James Jebaseelan Samuel, E., & Roopan, S. M. (2019). Chapter 12 - Nanoparticle characterization techniques. *Green Synthesis, Characterization and Applications of Nanoparticles*, 303–319. doi: 10.1016/b978-0-08-102579-6.00012-5
- Wagner, W. R. (2020). Chapter 1.3.1 — The Materials Side of the Biomaterials Relationship. In W. R. Wagner, S. E. Sakiyama-Elbert, G. Zhang, & M. J. Yaszemski (Eds.), *Biomaterials Science (Fourth Edition)* (pp. 83–84): Academic Press.
- Williams D.F. (2008) - On the mechanisms of biocompatibility. *Biomaterials.*; 29:2941–2953. - 10.1016/j.biomaterials.2008.04.023.
- Williams, D. F. (2019). Specifications for Innovative, Enabling Biomaterials Based on the Principles of Biocompatibility Mechanisms. *Frontiers in Bioengineering and Biotechnology*, 7. doi:10.3389/fbioe.2019.00255
- Yoshimura M, Noma T, Kawabata K, Somiya S (1987) Role of H₂O on the degradation process of Y-TZP. *J Mater Sci Lett* 6:465
- Zhang, Y., Shao, D., Yan, J., Jia, X., Li, Y., Yu, P., & Zhang, T. (2016). The pore size distribution and its relationship with shale gas capacity in organic-rich mudstone of Wufeng-Longmaxi Formations, Sichuan Basin, China. *Journal of Natural Gas Geoscience*, 1(3), 213–220. doi: 10.1016/j.jnggs.2016.08.002
- Zindani, D., Kumar, K., & Paulo Davim, J. (2019). Chapter 4 — Metallic biomaterials — A review. In J. P. Davim (Ed.), *Mechanical Behavior of Biomaterials* (pp. 83–99): Woodhead Publishing.

1. https://www.uobabylon.edu.iq/eprints/publication_12_1581_1707.pdf
last accessed March 29, 2022
2. <https://www.britannica.com/science/allotropy>
last accessed April 11, 2022
3. <https://www.unl.edu/ncmn-cfem/xzli/em/semoptic.htm>
last accessed March 29, 2022